LA-UR ~~10-~~ 11-00535

Approved for public release;
distribution is unlimited.

Title:	Unit Physics Performance of a Mix Model in Eulerian Fluid Computations
Author(s):	Erik Vold, XCP-2 Rod Douglass, XCP-1
Intended for:	Unclassified proceedings of the NECDC 2010 Conference, October, 2010 Los Alamos, NM.

Form 836 (7/06)

Unit Physics Performance of a Mix Model in Eulerian Fluid Computations.

Vold, E. (XCP-2) and Douglass, R. (XCP-1)
Los Alamos National Laboratory

Abstract

In this report, we evaluate the performance of a K-L drag-buoyancy mix model, described in a reference study by Dimonte-Tipton [1] hereafter denoted as [D-T]. The model was implemented in an Eulerian multi-material AMR code, and the results are discussed here for a series of unit physics tests. The tests were chosen to calibrate the model coefficients against empirical data, principally from RT (Rayleigh-Taylor) and RM (Richtmyer-Meshkov) experiments, and the present results are compared to experiments and to results reported in [D-T]. Results show the Eulerian implementation of the mix model agrees well with expectations for test problems in which there is no convective flow of the mass averaged fluid, i.e., in RT mix or in the decay of homogeneous isotropic turbulence (HIT). In RM shock-driven mix, the mix layer moves through the Eulerian computational grid, and there are differences with the previous results computed in a Lagrange frame [D-T]. The differences are attributed to the mass averaged fluid motion and examined in detail. Shock and re-shock mix are not well matched simultaneously. Results are also presented and discussed regarding model sensitivity to coefficient values and to initial conditions (IC), grid convergence, and the generation of atomically mixed volume fractions.

Introduction

In many computational applications involving fluid mixing due to turbulence or fluid instabilities, the full range of fluid scales cannot be resolved. It is common to represent small scale mixing with a model while the computational simulation resolves mixing at the large scales [2]. The mix models incorporate one or more coefficients, which must be set by comparison to experimental data, preferably in unit physics tests where each coefficient can be set independently [3]. As discussed in the next section, methodologies for calibrating multiple coefficients simultaneously in mix models are varied and not standardized.

The K-L drag-buoyancy model

The K-L drag buoyancy mix model considered here is detailed in [D-T], and the equations are summarized in the Appendix for reference. Starting with the compressible fluid equations supplemented with a species continuity equation, the mix model can be considered to include four components. One, additional terms in the mass averaged flow and species equations produce 'mix' by modifying the resolved flow in the computation. These new terms depend on the turbulent quantities, K (turbulent kinetic energy) and L (turbulent scale length). Two, evolution equations are solved for K and L on the

computational grid. Three, closure relations for terms in the K and L equations, use coefficients which are adjusted to fit empirical data. Four, self-similarity analysis further constrains the remaining model coefficients. The self-similarity analyses apply rigorously in the Lagrange frame of the mass averaged fluid, and in the limit as Atwood number, A, goes to zero. The results discussed later, suggest that these restrictions may be important and do not apply in all applications.

Analysis in [D-T] combines self-similarity constraints with empirical results to prescribe the model coefficients as summarized in their Table 1. The principle empirical constraints are derived from experiments in Rayleigh-Taylor (RT) mix [4-8] and experiments in Richtmyer-Meshkov (RM) mix [5, 6, 9-12]. The constrained coefficients are incorporated into the drag-buoyancy source term to the K evolution equation (see Appendix). In RT mix experiments, the mix layer width grows as $h = \alpha A g t^2$, where α has been observed in the range 0.05 – 0.08 [4, 13, 14]. The value of $\alpha = 0.06$ is chosen by [D-T] and in combination with other coefficients, this sets the K-L buoyancy coefficient, $C_B = 0.84$.

In single shock RM experiments, late time mix layer growth verses time is often fit to a power law [6, 15, 16]. This growth is expressed in a form, $h = h_o(1 + t\, v_o/(h_o\theta))^{\theta}$ in order to fit data to initial conditions for perturbation scale length, h_o, and initial mix velocity, v_o, in addition to the exponent for late time growth [6]. The power law exponent reported in the literature has a substantial range, typically, $\theta \sim 0.2 - 0.5$ [6,15,16]. In [D-T], the value of $\theta = 0.25$ is assumed to apply for small Atwood numbers, and this is used to set the model drag coefficient, $C_D = 1.25$. This value of the model drag coefficient is also consistent with the decay of HIT (homogeneous isotropic turbulence), which is experimentally observed in some cases to follow nearly linear decay in time [17]. A self-similarity analysis [D-T] is then used to constrain the additional model parameters.

The coefficient for the turbulent diffusivity, C_T, is unity in this model, consistent with the self-similarity constraints. The coefficient value cannot be set in the usual way against KH (Kelvin- Helmholtz) instability or shear layer mix growth [18] until the deviatoric source terms in the turbulent stress are included in the model. This in turn requires a shock-stable form for those terms, and would then require rescaling the diffusion term coefficients terms as described in [D-T].

The turbulent diffusivity coefficient is 'classically' determined by comparing to K-H instability growth [18] and is then found to be ~ 0.1. In an independent calibration study of a similar K-L drag-buoyancy model [19], Chiravalle uses a different methodology to set the model coefficients, wherein the RT, RM and KH empirical mix rates were used simultaneously to set the three principle model coefficients, C_B, C_D, and C_T. That study found the turbulent drag coefficient to be 0.3, however, the drag source term there is normalized differently than in [D-T], so a direct comparison, assuming the [D-T] form of the drag term, would put the Chiravalle coefficient at $C_T \sim 0.15$, close to the classical value. In another recent mix model calibration, a version of the BHR mix model [20] (which is also a K-L based turbulent mix model) found $C_T = 0.56$ [21]. The range in

these results suggests there is no single accepted calibration methodology, nor a universal value for turbulent diffusion across turbulence models.

To evaluate the K-L drag-buoyancy mix model implementation within an Eulerian code, the unit-physics tests are adapted from [D-T]. In that study, the mix model is implemented within an ALE code and the tests were run in a pure Lagrange mode [22]. That allows a direct comparison between the model results within the computational code and the expectations from the self-similarity analysis, which sets the model coefficients in a Lagrange frame analysis. The model as summarized in the Appendix, is written in terms of the convective derivative for all convected quantities, and in that sense it is cast in a Lagrange form. In the present study, the K-L model has been implemented within an Eulerian code [23], and some mix model results which will be shown to differ from the previous work may be attributed to this basic difference in formulation of the underlying computational framework.

Model coefficient default values used here are the same as given in Table I of [D-T]. These include the three principle values, as discussed above, of $C_B = 0.84$, $C_D = 1.25$ and $C_T = 1$. The values of the turbulence variables, K and L, evolve from initial values, K_o and L_o, which are specified as model inputs, and then used by the code to initialize K and L at all material interfaces in the problem. Results will be shown to depend upon these initial values, so these are considered as additional model parameters.

Eulerian Implementation

The algorithm in the Eulerian fluid computation used in this study is based on work by Scannapieco [23]. It can be considered as a Lagrange phase projection with a full advective re-map back to the original grid, similar to that described in [24-26]. The Lagrange phase and internal energy require an artificial viscosity to stabilize numerics and to better maintain total energy conservation in the presence of shocks. [25]. The computational grid is rectilinear and all tests are run in 1-D geometries. An AMR (adaptive mesh refinement) capability is turned off to force the test problems to run on a uniform grid in order to reduce possible numerical instabilities.

Interfaces between different materials are tracked with a VOF scheme [27]. As materials mix, an unmixed volume fraction for each material evolves to an atomically mixed fraction in proportion to the material volume fluxed by the mix velocity [23]. This mix velocity is based solely on the turbulent diffusivity in the species mass equation. However, the K-L model also modifies the mass averaged velocity, u, through the gradient in K, and then the mix width may be modified by this change in u, in addition to the atomically mixed fraction generated by the species turbulent diffusion flux. The unmixed fractions are used to maintain a 'quasi-interface' for VOF, even as mixing evolves, while the mixed fractions (denoted 'atomically mixed volume fractions' in the results section) can be used to define mixed volumes for computing reaction rates between reactive mixing materials.

Test Method Basics

'Mix' is evaluated as a width or thickness of the mixing fronts verses time in this and in the reference study, using in most of our cases, the 5% and the 95% variations in the volume fractions of the two mixing materials. In many tests, mix width is evaluated separately for the bubbles (light fluid) and the spikes (heavy fluid) relative to the position of the unmixed contact discontinuity. This position moves significantly through the computational mesh for the RM mix cases. Only binary mixing and 1-D tests are considered in this study.

Results

RT mix

The RT problem set-up follows that given in [D-T], with imposed acceleration, g = $0.00098\ cm/\mu sec^2$, and ideal fluids each with heat capacity ratios, $\gamma = 5/3$. Fluid densities are constant initially, with fluid one density, $\rho_1 = 1\ g/cc$, and the density of fluid two is varied in different runs to set the desired Atwood number. Initial hydrostatic equilibrium is set with a linear variation in internal energy in each fluid region. Pressure at the fluid interface is set to be consistent with fluid temperatures of 1 eV. Default K-L model parameters were used and the initial values were chosen *as* $K_o = 1.e\text{-}8\ g\ (cm/\mu sec)^2$, and $L_o = 1.e\text{-}5\ cm$. A range of IC values were evaluated and gave similar results.

A large suite of runs was examined. An example of results showing self-similarity of the profiles of K across the mix layer during RT mix are given in Figure 1, for two of the cases examined, with Atwood numbers of 0.05 and 0.8. The results agree with those in [D-T], and show the important characteristic of near symmetry at low A, and increasing asymmetry at high A, with the profile leaning in the direction of the 'spikes' from the heavier fluid. This self similarity is essential to recover the desired RT growth rate proportional to t^2, where the velocity grows as the gradient of $K \sim K/L$, and therefore both K and L must exhibit self-similarity to maintain this constant ratio defining the mix acceleration during the mix evolution. Self-similarity in the growth of the turbulent length scale, L, was also demonstrated (not shown).

The mix layer growth and its variation with grid resolution is shown in one example for $A = 0.8$ in Fig.2 (top). Mix growth appears linear with Agt^2 as expected. In plots (not shown) of the mix width verses time on a log-log scale it is apparent that the mix width grows in time with an exponent slightly less than two (~ 7/4). The convergence behavior will be discussed later in the section on *Grid Convergence*.

Results for the RT growth rate, alpha, $\alpha = h/Agt^2$, are summarized in Fig.2 (bottom panel) for the full range of Atwood numbers on converged grids. This growth rate matches the previous results in [D-T] closely and shows good agreement with experiments [4-6], where alpha for the bubbles is near 0.04-0.06 and approaches 0.06 at low A, while alpha for the spikes increases significantly from ~ 0.06 as A increases. This trend across A is in good agreement with previous work [6,13].

HIT (Homogeneous isotropic turbulence)

A simple HIT setup assumes a 1-D problem with all zones mixed so that each zone is initialized to the prescribed K and L initial conditions, K_o and L_o. We confirmed that the results are identical in any of the 1-D problem zones, as they should be. In these tests, L_o is set to 1.e-4 cm, and K_o is set to either $K_o = 1.e\text{-}5$ or to $K_o = 1.e\text{-}8\ (cm/\mu sec)^2$. These two values of K_o correspond loosely to initial conditions defined to be 'turbulent' or 'quiescent' relative to the thermal energy in the problem, as described in the later section on *RM mix sensitivity to IC.*

Our test results are shown in Figure 3, for the time dependence of the model turbulent kinetic energy, K[t] and the turbulent scale length, L[t]. The decay of K fits a power law with exponent, $\theta \sim -1.12$, while L grows with power law exponent, $\gamma \sim 0.43$. These results are independent of the initial value of K_o after an early time transient. These results are in excellent agreement with the expected values from the self-similarity analysis in [D-T] of $\theta \sim 1.1$, and $\gamma \sim 0.44$ appropriate for the value of the drag coefficient, $C_D = 1.25$. The decay of homogeneous isotropic turbulence has been studied extensively and it has been shown in analyses that the decay of turbulence should be linear in time [17]. This agrees to within 10% with the self-similar result, $\theta \sim -1.1$ as given in the analysis of [D-T].

RM mix

Shock set-up

Shocks of specific magnitude are generated using the polytropic gas relations for shocks into initially stationary fluids [28]. A shock impinges on a contact discontinuity in the RM mix tests, in which the Atwood number is defined by convention as positive for a step up in density at the contact discontinuity and negative for a step down in density. Thus, for the shock moving from fluid 1 to fluid 2, the Atwood number is

$$A = \frac{(\rho_2 - \rho_1)}{(\rho_2 + \rho_1)}$$

Initially, the shock front was specified a distance upstream from the initial contact discontinuity (CD) to reproduce the tests as shown in [D-T]. However, this allowed a significant time before the shock reached the CD and the mix model produced a small but significant amount of mixing prior to the arrival of the shock. To avoid this undesirable early time pre-shock mixing by the model we set the shock front to be adjacent (one zone upstream) to the CD interface in subsequent tests.

The 'base case' in the RM shock studies used the shock described by [D-T] in section VI, with Mach = 1.57, V_{shock} = 0.022 cm/μsec, and shock density = 1.812 g/cc, impinging on an ideal gas of density 1 g/cc and $\gamma = 5/3$. Density and internal energy, respectively, in fluid two are adjusted to set A, and to maintain pressure equilibrium at the CD. The initial conditions for K_o and L_o in these tests are not specified in [D-T].

RM Mix Sensitivity to Initial Conditions (IC)

Extensive studies to explore the basic response of the model to shocks indicated the model results for RM mix are sensitive to the initial conditions for K and L, specified in the input values, K_o and L_o. Select results from the studies are summarized in Figure 4, showing the mix width for A = - 0.2, evaluated separately for bubbles and spikes, for several combinations of initial conditions for K_o and L_o. It was found that below a certain threshold for K_o, the results were independent of K_o, for example comparing K_o = *1e-12* and K_o = *1e-8 (cm/μsec)*^{2}. Above this threshold, the mix width increases significantly with K_o, as seen comparing K_o = *1.e-8* and K_o = *1.e-5* cases. The threshold value, here $K_o \sim$ *1e-5*, is interpreted as distinguishing initial conditions which are 'quiescent' *(K_o << 1.e-5)* from initial conditions which are 'turbulent' *($K_o \geq$ 1.e-5)*. This threshold defining the 'turbulent IC' corresponds to a turbulent kinetic energy of a few percent of the thermal energy in the problems run here.

In figure 4, the RM mix width for two cases of L_o = *1.e-2* and L_o = *2.e-2 cm*, shows a strong and direct dependence on L_o. We have found that varying L_o is a convenient way to match mix widths in various RM experiments, typically in the range reported here $L_o \sim$ *(1 – 2) e-2 cm*. This range is compared to the value of $L_o \sim$ *1.e-5* used as IC in the RT studies. Since the RM mix results are clearly sensitive to the initial values for K and L, these specified input values, K_o and L_o, should be considered as additional parameters in the mix model.

RM single shock, varying Atwood numbers

Mix width growth is shown in a composite of cases in Fig. 5 *for A = +/- 0.2* and for *A = +/- 0.8*, with bubble and spike widths evaluated separately. In this case, the mix front positions, indicated by volume fractions of 1 % and 99 %, are evaluated in relation to the position of the unmixed interface in the same shock conditions. As expected in comparison to results in [D-T] and in experiments (e.g., [6]), the spikes grow slightly faster than the bubbles at the lower value of A, and there is a large spike to bubble difference at the higher Atwood numbers. The fitting coefficients, *m1, m2, m3* in the power law fits for mix width, *h*, verses time, *t*, are related to the form proposed in [D-T] as,

$$h = h_o\left(1.+\frac{t\ v_o}{\theta\ h_o}\right)^{\theta} = m1(1.+ m2\ \ t)\text{^}m3 \qquad (1)$$

where, h_o, is the initial condition for a perturbation scale length, v_o, is an initial mix velocity, and θ is the exponent for late time growth. (In the examples in Fig.5, there is also an initial time shift, fit as *m4*, but this does not influence the results for the other parameters.) The power law exponent, *θ*, fit to the model parameter, *m3*, is found to be 0.37 – 0.39 in the cases in Fig. 5 with the smaller Atwood number, with a small difference between the bubble and spike values. At *A = 0.8*, the exponent, *θ = m3 ~ 0.42* increases for the bubbles and *θ = m3 ~ 0.49 – 0.51* and for the spikes. These values are significantly higher than expected, *θ ~ 0.25,* for the bubbles based on the self-similarity calibration methodology in [D-T]. The results in figure 5 are representative, and

consistent with many other tests not shown, where the power law exponent for late time RM mixing falls in the range $\theta \sim 0.3 - 0.5$.

RM sensitivity to drag coefficient, C_D

This difference in the power law exponent obtained here and in the previous Lagrange based calculations in [D-T] prompted investigation into the sensitivity of the RM mix results to the drag coefficient, C_D. This drag coefficient was varied from the default, $C_D = 1.25$, to values as shown in Figure 6. The top panel shows the resulting fits for the bubble mix widths using a standard two-parameter power law. The bottom panel shows the improved fits from the three-parameter power law model (given in the equation above). A small dependence of the mix width on the drag coefficient is seen in the figures. The power law exponent has a small variation with C_D, and it appears to be less sensitive in the two-parameter fit than in the three-parameter fit. A comparison is plotted in Figure 7 (top panel), showing the theta value best fit to the mix model width verses the specified drag coefficient, for both the 2 and 3 parameter power law fits.

There were several additional runs varying the drag coefficient, and examples are shown in Fig. 7 (bottom), where bubble and spike growth over a long mix time are compared to the total mix width growth over a short mix time. The results are similar and show a weak sensitivity of mix exponent to the drag coefficient value. This is in contrast to the significant sensitivity observed in [D-T] as shown in their figure 24, where theta varies from ~ 0.6 down to ~ 0.24 over the same range of C_D shown here. In our test runs at lower Atwood number (A = 0.02, not shown) we found the smallest theta value to be, $\theta \sim 0.28$, for $C_D = 2.5$, however at the default drag coefficient of $C_D = 1.25$, the resulting fit for theta at A = 0.02 was found to be, $\theta \sim 0.4$. We will return to discuss model sensitivity to drag in the section on *K-L model sensitivity to a uniform flow velocity.*

RM re-shock 1 – Vetter-Sturtevant experiment

The K-L mix layer growth rate was evaluated for the Vetter-Sturtevant [V-S] experiment [11], using similar set-up and IC as given in [D-T], where the V-S experiment # 85 was modeled. A Mach = 1.5 shock impinges on an air-SF6 interface (A ~ +0.67). This required reducing the ambient pressure at the CD to obtain this Mach number in the experiment. Two experimental runs (85 and 90) are reported in [11] for this same Mach number where the difference is only in the details of the mylar-wire-mesh interface used to establish the discontinuity of the IC. The experimental results were sensitive to the IC in ways not well understood, and not easily modeled [29].

Mix model results are compared to experimental results in Figure 8. A large difference between the two experiments due to the IC is evident. With the default model parameters set, the initial conditions can be varied to best match the data. Two cases for the K-L model results are also shown in comparison, with $L_o = 0.127$ (as in [D-T]), and using a larger value, $L_o = 0.4$ The model can match either the early time single shock RM mixing or the later time re-shock mixing by adjusting the initial turbulent scale length, L_o. It appears unlikely that a single set of initial conditions with the default model parameters can simultaneously match the mixing following the first shock and simultaneously match the mixing after re-shock. This is in contrast to the results reported in [D-T] where good

agreement was obtained in the first shock and in the re-shock mixing with the same model parameter values used here. The different results may be related to the relative insensitivity to the drag coefficient seen in the Eulerian implementation of the model.

RM re-shock 2 – Poggi, et.al. experiment

The Poggi, et.al [Poggi] experiment [12] involves a Mach = 1.45 shock initiated in SF6 and propagating across an SF6-air interface *(A ~ - 0.6)*, and then reflecting from a shock tube end-wall to re-shock the SF6-air interface from the air side. The K-L mix layer growth rate was evaluated for the Poggi experiment using similar set-up, IC, and model parameter settings as given in [D-T]. The model results for the mixing front positions are compared to a sub-set of the experimental data in Fig. 9 (top) and the front positions are used to determine the mix widths verses time in Fig. 9 (bottom). The top figure shows a reasonably good overall match to the experimental mixing front positions, however, the bottom figure shows that the mix width for each model case is in poorer agreement with the experiment. It is interesting to note that the default model settings (labeled 'base' in the figure) match the first shock mix and under predict the re-shock mix, and this result is nearly identical to that reported in [D-T] with the same default model parameter values. However, they were able to obtain a good fit to both mix regimes simultaneously by adjusting the parameters far from their calibrated default values. In our results, even with modified coefficients, we were unable to match the mixing in both regimes simultaneously. Again, this difference may be related to the observed insensitivity to the drag coefficient, C_D, seen in the Eulerian model implementation.

In addition to data on mix front verses time, the Poggi experiment provided data on turbulent fluctuation levels, measured at several locations as an average of the axial variance, $\langle u_x^2 \rangle$. This data is compared directly to Lagrange results in [D-T], and can be compared to results in the Eulerian frame by converting the time axis to distance using the shocked fluid mean velocity. The results for fluctuations, evaluated as 2K in the model, are shown in Figure 10, and these can be compared qualitatively to the results in [D-T] or in Poggi [12]. The magnitudes of the model fluctuations are small compared to the experimental data for axial fluctuations by a factor of 2 to 4. Anisotropy in the experimental fluctuations might account for much of this difference but the anisotropy was not measured and so it cannot be quantified. The model results here agree with the previous model results [D-T], to within a few tens of percent at most location/times but only within about a factor of two at the location of the peak fluctuations, where the greatest difference between model results is seen. However, at this same location, agreement of either model with experiment is best; the previous Lagrange based computations agreed with experiment to within about 50%, and the present model implementation agrees with experiment to within a factor of about two.

Shock amplification of turbulent kinetic energy

An experiment by Barre, Alem, and Bonnet [30] (denoted BAB) examined the shock amplification of turbulent kinetic energy by measuring fluctuation levels in the interaction of a normal shock with homogeneous turbulence. Air is driven in a wind tunnel through a mesh which generates an initial homogeneous turbulence field and then propagates downstream past fixed obstacles which set up a Mach = 3 standing shock

wave in the turbulent air. Hot wire anemometry and laser Doppler velocimetry are used to measure axial fluctuations, the decay of anisotropy in the fluctuations after passing the shocked surface, and also a longitudinal integral turbulent length scale.

The complex experiment is modeled in a simple way, with mixed materials prescribed in all zones, which initializes the turbulence in the K-L model everywhere to K_o. A Mach = 3 shock is launched and the fluctuation levels, K, relative to the pre-shock initial values are determined as a function of distance from the initial shock front, at sufficiently late times to span the experimental domain. The model values for amplification of K, post-shock to pre-shock values, are compared to the experimental post-shock to pre-shock values for amplification of the longitudinal fluctuations in Fig.11. The initial decay of the anisotropy, seen in the experimental data out to a distance of about one cm, cannot be represented in the isotropic turbulence, K, in the model. The experimental amplification values are near a factor of three shortly after the shock passes, in reasonable agreement with the model (ignoring a very brief transient amplification of about 6 seen in the experiment). After the experimental value decays to the axisymmetric late time value of about 1.5, (where the anisotropic ratio of longitudinal to transverse fluctuations is also equal to 1.5) then the model result is almost a factor of two greater than the data. If the anisotropy is factored in as described in [D-T] then the average K post-shock to pre-shock values consistent with the experiment are expected to be even smaller and so the discrepancy with the model result would be greater. Model results reported in the Lagrange work [D-T] were in better agreement with the experiment but still overshot the data by about 40% at the point with the best agreement, and by a larger margin at other locations.

Grid Convergence Studies

Results of the K-L mix model in the base RM mix problem, with $A = -0.2$, were compared on varying grid resolutions to determine grid convergence. An example is shown in Figure 12 (top), where mix width verses time on a log-log plot indicate the power law dependence is not changing significantly while varying grid resolution from $dx = 0.008$ down *to* $dx = 0.00025$ *cm* or 2.5 microns. Note that the mix width decreases as grid size decreases. In analyses (not shown here) it was determined that the K-L model result for the RM problem is converging 'better than linearly', meaning the normalized change in solution per change in resolution scaled approximately as: dx^{γ} with $\gamma = 1.2$. This is evaluated assuming the solution on the finest grid is the 'accurate solution', then plotting a difference in the solutions, each course grid solution minus the finest mesh solution, against the course grid resolution, expressed as $1/dx$. The slope (on a log-log plot) then indicates a measure of the convergence rate with resolution and was found to be $\gamma = 1.2$. Convergence errors are quantified further in the next section.

For comparison, we examined the grid resolution in an alternate mix model, the multi-fluid interpenetration mix model reported in Scannapieco-Cheng [31]. The mix in this model is driven by the species pressure gradients at fluid interfaces, and so an interfacial pressure gradient driven mix problem is used to test the convergence. In our tests, two different fluids of the same density (1g/cc) each occupy half of a one cm. domain. Fluid temperatures are initialized at 2 keV and temperature exchange appropriate to this dense

plasma regime is included. Mix results from this model have similar characteristics across a range of test problems, indicating the results here are representative of other problems. The mix characteristics from this model are not explicitly sensitive to the type of instability expected at the fluid interface.

Mix results for the Scannapieco-Cheng [31] model are summarized in Fig.12 (bottom panel) as a mix width verses time for a range of grid resolutions. The most course grid just barely resolves the domain, while the finest grid at 25 microns has 400 zones across the domain. The mix width growth approaches a linear phase at late times, and the slope approaches a constant value on the finer grids indicating a convergence for the linear mix rate. Note that the mix (width) increases in going to the finer grids. This is presumably attributed to the mixing drive in the pressure gradient drive term, where the numerical approximation to the pressure gradient scale length is limited by the finite grid resolution, and thus the pressure gradient driving mix can increase as dx decreases.

A grid resolution comparison is summarized in Fig. 13, which includes the K-L model results in the RT problem (taken from Fig. 2), the K-L results for the RM problem (Fig. 12 top), and the interpenetration mix model results for the pressure gradient interfacial mixing problem (taken from Fig. 12 bottom panel, and denoted 'trbf1 in grad(p1)' in Fig.13). The plot reflects a fractional error each time the grid is refined by a factor of two. It shows the relative change at a late time in the mix width, h, plotted against grid resolution, dx, with the relative change on two grids, evaluated as $((h(dx_i) - h(dx_{i-1}))/h(dx_i)$ where dx_i is the courser grid size and dx_{i-1} is the next finer grid, and is half the grid size of dx_i. This allows a simple convergence comparison of each mix model in a type of test problem appropriate to that model.

The K-L mix model results change across grid resolutions by less than 40% per halving dx in the RM problem, and less than 20% change in halving dx in the RT problem on the course grids, and with much smaller changes as dx approaches zero. The largest dx examined in the RT problem was 100 microns but the result suggests that K-L converges in RT at least as well as in RM on grids with *dx* up to a few hundred microns. On the course grids, the interpenetration model [31] in the pressure gradient test problem, denoted 'trbf1', had the largest relative change in the solution, of almost 100% between the course grids, indicating poor convergence at the course resolutions. At grids of 100 microns and finer, this model solution changed only slightly indicating good convergence at the finer resolutions. The good convergence at the fine grid may be related to resolving the species pressure gradients adequately at those resolutions. It may also be related to better resolution of the energy exchange, which depends upon temperature gradient scale lengths limited by the grid resolution in the numerical approximations.

K-L model sensitivity to a uniform fluid velocity

The discrepancies in the RM power law exponent and its sensitivity to the drag coefficient seen between the present Eulerian implementation of the K-L model and the results in the Lagrange computations [D-T] prompted further study. Possible differences exist in the effective fluid drag as seen in the Eulerian frame compared to the Lagrange frame used in the self-similarity analysis to set the model coefficients. The Lagrange

frame convective derivative for K (see Appendix) is assumed related to the scale length, L, and the drag-buoyancy source term, $S_K[K,L]$, a function of K and L. In a simplified form the K evolution equation is

$$\frac{DK}{Dt} = \frac{\partial K}{\partial t} + u \cdot \nabla K \sim \frac{\partial K}{\partial t} + u\frac{K}{L} \sim S_K[K,L]$$

The convective term, $\sim u\,K/L$, is irrelevant in the Lagrange frame but can modify the evolution of K if (K/ L) evolves similarly as u varies. This is expected to be true when u represents a uniform background motion, u_o, if the value of u_o is varied between different test cases.

To test this, a simple contact discontinuity (CD) in pressure equilibrium (the same used in the RM mix problem) was re-run while varying a uniform background flow velocity, u_o. There is no shock, to avoid differences due to the shock impinging on the CD at different velocities, so the mix layer forms only in response to the decay of K from its initial value. In this problem, $A = -0.2$, $L_o = 1.e\text{-}2$ and two initial values of K are compared, $K_o = 1.e\text{-}8$ (quiescent IC) and $K_o = 1.e\text{-}5$ (turbulent IC) as introduced in Fig. 4. A uniform background flow velocity, u_o, is imposed defining three cases as: $u_o = 0$ (denoted u00), $u_o = 0.01$ (u01) *and* $u_o = 0.02$ (u02), where case u01 corresponds to Mach ~ 0.7 and u02 corresponds to Mach ~ 1.4, relative to the sound speed of the heavier fluid at the CD.

The mix widths for these six cases are shown at select times in Figure 14 (top). It is evident the mix width increases with the velocity of the uniform background fluid for either value of K_o. This is in contrast to the hypothesis that the increased convective flow in the Eulerian frame might create an effective drag, increasing the drag over that intended in the Lagrange frame model, and thus decreasing mix with increasing background fluid velocity. To examine this further, the model kinetic energy, K, is plotted verses time in Fig.14, separately for the two K_o values, for $K_o = 1.e\text{-}8$ (center panel) and $K_o = 1.e\text{-}5$ (bottom panel). Kinetic energies at different background velocities differ significantly at early time, but tend to converge at late times. The differences are greater for the 'quiescent IC' (middle panel) than for the turbulent IC (bottom panel), and the differences are greater between $u_o = 0$, and $u_o = 0.01$, than between $u_o = 0.01$ and $u_o = 0.02$.

In expanded plots (not shown) it is evident at late times, especially in the quiescent IC cases, that K does decay faster and to smaller values at a given time as u_o increases. This late time behavior is consistent with an increase in the effective drag in proportion to u_o, the convective flow, as hypothesized above. However, if the early time differences in K dominate the mix width behavior, then the early time K drives a larger initial mix velocity, v_o, with increasing uniform flow, u_o. It appears this effect is greater than the increase in effective drag at late times. With this interpretation, the behavior of K appears consistent with the mix widths seen in the Fig.14 top panel. It is not clear if this sensitivity to a uniform flow is a shortcoming of the mix model in an Eulerian frame, or if

it results from details of the numerical implementation. This issue might be worth examining in future work.

Sensitivity to turbulent diffusivity, C_T

As a practical matter, it is desirable to be able to vary the turbulent diffusivity coefficient to match experiments, and so we examine the sensitivity of the model results to variations in the key parameter, the turbulent diffusivity, C_T. It is recommended in [D-T] that if the value of C_T is changed, then the self-similarity coefficients must be reset consistently. However, in these tests, the similarity coefficients, N_s, are left at the default values to examine the impact of varying C_T alone.

Mix width for the base case RM instability (*Mach = 1.57*, and $A = -0.2$) is compared in Fig. 15 (top), for the default value *of* $C_T = 1.0$ and the 'usual' value calibrated against K-H shear layer mixing [18,19] *of* $C_T = 0.1$. The mix width at a late time differs by 27% between these two cases. As the turbulent diffusivity decreases further below $C_T = 0.1$, there is no further significant change in the mix width at late times (this is not shown, as the volume fraction curves overlie each other for values of $C_T < 0.1$). However, there is a change in the 'atomically mixed volume fraction', seen as 'af.1' in Fig.15 (bottom). This quantity continues to decrease in proportion to the value of C_T as shown in the figure down to $C_T = 0.01$.

These results show that by varying only the turbulent diffusivity, the mix width and the atomically generated mix fraction become weakly coupled for small diffusivities. Referring to the model equations in the Appendix, the mix widths (or effectively, the profiles of mixed material total volume fractions, Vf) are controlled by a combination of the gradient of K in the momentum equation and the turbulent diffusivity in the species mass fraction equation. It appears that the diffusivity contribution to the mix width becomes negligible as C_T is decreased below $C_T \sim 0.1$. On the other hand in this Eulerian implementation, the atomically mixed volume fraction is generated directly and only by the turbulent diffusive flux in the mass species equation, and so it depends on C_T down to arbitrarily small values. This is a reasonable consequence of the spread in interfacial density by the mass averaged velocity driven by the gradient in K, while the diffusive mass contribution to the interfacial density profile becomes negligible as C_T approaches zero.

The profiles through the mix layer for the total volume fractions for materials 1 and 2, vf.1 and vf.2, are compared to the atomically mixed fractions, af.1 and af.2, in Fig. 16. Also indicated are simple sums and products of these volume fractions which might be used to accurately determine the reaction rate between initially unmixed reactants in the two mixing fluids. This distinction between the material volume fraction and that portion of the material volume fraction, which is actually atomically mixed, is critical to understand and to accurately predict reaction rates in reactive fluids. Mixing can produce small scale mix structures with very little actual atomic mix when the diffusivity is small, or it can produce large atomic mix fractions when the diffusivity is large. For example, a detailed model which distinguished the sub-grid structured mix from the atomic mix, was described recently [32]. Details of the sub-grid mix components are tied into the

numerical representations of the interface between the fluids, the numerical model for fluxing masses and volumes of fluids across that interface, and the way the equations of state for mixtures and pure fluids are treated. These topics will be explored in future work.

Discussion and Summary

A K-L turbulence mix model driven with a drag-buoyancy source term was tested in an Eulerian code in a series of basic unit-physics tests. The model and the closure coefficient values are derived in the work of Dimonte-Tipton [1]. Many of the test problems were reported there, where the mix model operated in Lagrange computations. For the present work, the drag-buoyancy K-L mix model was implemented within an Eulerian code framework by A.J. Scannapieco [23]. Mix model performance is evaluated in terms of mix width growth rates compared to experiments in select regimes, and compared to the previous Lagrange computational results reported in [D-T]. Results in the Eulerian code mix model are presented for several unit-physics 1-D test problems including the decay of homogeneous isotropic turbulence (HIT), Rayleigh-Taylor (RT) unstable mixing, shock amplification of initial turbulence, Richtmyer-Meshkov (RM) mixing in several single shock test cases and in comparison to two RM experiments including re-shock (Vetter-Sturtevant and Poggi, et.al.).

Sensitivity to model parameters, to Atwood number, and to initial conditions (IC) were examined. Results here are in good agreement in some tests (HIT, RT) with the previous results reported for the mix model in the Lagrange calculations. The HIT turbulent decay agrees reasonably well with analytic expectations, and the RT growth rates match experimental values using the default values of the model coefficients proposed in [D-T]. Results for RM characterized with a power law growth rate exponent differ from the results in previous mix model work but are still within the range for reasonable agreement with experiments and other models in the literature [6, 15,16]. The larger power law exponent in the present Eulerian code implementation is also relatively insensitive to variations in the drag coefficient.

These tests indicate that the Eulerian code K-L model, using the Dimonte-Tipton default model closure coefficients, achieves reasonable results across those unit-physics tests where there is no net flow, i.e., where the mass average flow in the Lagrange convective derivative is zero. The mix model results differed in the Eulerian code implementation from those previously reported in the Lagrange frame in [D-T] for the shock driven flows (RM) where the mix layer is moving through the computational grid.

These findings suggested a possible increase in the effective drag coefficient in the fixed Eulerian frame relative to the Lagrange frame moving with the fluid. Additional tests varied the speed of a uniform background fluid flow in the Eulerian frame. These showed a sensitivity to the background flow speed, with differences in the mix width and in the early time values of the turbulent kinetic energy. At late times with the different uniform flow speeds, the turbulent kinetic energy converged toward a similar profile,

suggesting the differences are less strongly related to a late time difference in the drag but may be related to early time differences in the growth of the kinetic energy which increases the initial mix velocity in proportion to a uniform background flow speed. This can be related to the convective derivative of the kinetic energy as implemented in the Eulerian frame.

Initial conditions can be adjusted so that single shock RM mix width results match experiments but we have not been able to obtain a good match for first shock and re-shock growth rates in the same experiment with a single set of parameters and IC. Shock amplification of turbulence is compared to an experiment and the model results in this study compare well to the previous Lagrange calculations. In cases where turbulent fluctuations were measured in experiment, agreement with the model results was adequate, usually within a factor two.

Problematic issues with the turbulent diffusivity coefficient, C_T, exist as described in [D-T]. This coefficient is normally calibrated against Kelvin-Helmholtz (KH) shear test problems, but in order to achieve this, the viscous tensor must be numerically stabilized against shocks. A second concern is that if the coefficient value is modified in this mix model, then the self-similarity analysis must be repeated to reset other model coefficients consistently. An alternative calibration methodology, which avoids the limits imposed by the self-similarity, would be to calibrate the three principle model coefficients, C_B, C_D, and C_T, in the manner described in Chiravalle [19].

Sensitivity to IC values in the RM studies are examined. Results are sensitive to initial values of L[t=0], which largely determines the RM mix layer growth rate, and generally differs from the IC values used in the RT studies. Result sensitivity to initial turbulence, K[t=0], is seen to be small but significant above a threshold value. This 'threshold value' loosely distinguishes initially turbulent from initially quiescent fluid conditions relative to the thermal energy in the problem. It is reasonable to expect IC sensitivity in extrapolating to high energy density regimes. It is unclear how to best set IC in experiments with deceleration in arbitrary combinations of RT and RM, and a methodology for this needs to be developed in future work.

Resolution studies for an RM test problem show the K-L mix growth rate decreases as it converges at a supra-linear rate, and, convergence requires a fine grid (on the order of 10 microns). For comparison, a resolution study of the Scannapieco mix model [31] acting on a two fluid interface problem was examined. The mix in this case was found to increase with grid resolution at low to moderate resolutions, but converged at comparably fine resolutions. The atomically generated mix fraction and the mix width were compared for the K-L mix model and the Scannapieco model on an identical RM test problem (not shown in figures). In the Scannapieco model [30], atomic mix fraction and mix width grow linearly in time. The K-L model mix fraction and mix width are found to grow with a similar power law exponent. In future work, it is proposed to do more head-to-head comparisons between these two models and other mix model options on a full suite of physics test problems, such as the interfacial deceleration during an idealized ICF implosion, which introduces a complex combination of RT, RM and KH instabilities.

Generally, in a turbulence mix model, one expects to be able to adjust the turbulent diffusivity to accommodate experimental results. Atomically generated mix fractions were compared to the mix widths in the K-L model for variations in the turbulent diffusivity coefficient. This shows that for changes in diffusivity without resetting the self-similarity coefficients, there is a non-linear relationship between atomic fractions and mix width. Mix width is shown to be weakly sensitive to the diffusivity coefficient between values of 1 and 0.1, and independent of diffusivity below 0.1, while the atomic fraction is directly proportional to the diffusivity in the limit as the turbulent diffusivity approaches zero. Physically, this is reasonable and indicates that a very small diffusive mix will not change the bulk profiles significantly. However, this also indicates that within the present implementation of the mix model, profiles of the mix width are not a good indicator of atomic mixing in the limits of small diffusivity.

As a final point of discussion, the model results can be compared to the classic RM growth rate [9,10] expected in the early time linear phase of the RM mixing. The RM mixing layer thickness, h_{RM}, can be expressed as:

$$h_{RM} \sim 2\pi \frac{\delta_o}{\lambda_o} A\, v_i t$$

where δ_o is an initial perturbation amplitude, λ_o is the perturbation wavelength, and v_i is a post-shock interfacial velocity. The power law fits to the RM mix widths from the K-L model provide an estimate of the initial velocity, v_o, of the mix layer, given in the fitting equation (Eqn.1, p.6) to be $v_o = m1*m2*m3$. For example, using the results for the A = +/- 0.2 cases shown in Fig. 5, we find $v_o \sim 0.00055\ cm/\mu sec$, and in these cases the contact discontinuity was found to move with the post- shock interfacial velocity, $v_i \sim 0.01 cm/\mu sec$. These model results with the classic RM linear growth rate then set a unique ratio for the amplitude relative to the wavelength of the initial perturbation. Assuming $h_{RM}/t \sim v_{RM}[t=0] \sim v_o$, then in this example we find

$$\frac{\delta_o}{\lambda_o} \sim \frac{1}{2\pi}\frac{v_o}{A\, v_i} \sim \frac{0.00055}{2\pi\ 0.2\ 0.011} \sim\ 0.04\ -0.05$$

The model results for the early time linear growth are thus consistent with a specific ratio, (δ_o/λ_o), in the IC, in this case about 4 – 5 %. This is a reasonable value but it cannot be varied in the model to represent other ICs.

Conclusions

A K-L model with a drag-buoyancy source term for turbulent material mixing of fluids was implemented in an Eulerian hydrodynamic code, and in this report it is tested in a series of 1-D unit physics test problems representing several types of RT (Rayleigh-Taylor), and RM (Richtmyer-Meshkov) instabilities, and other simple flows. Model

performance is evaluated using the mix width verses time and in some cases the turbulent fluctuation levels. Results are compared with experimentally determined parameters and with the results previously reported in a reference study [1]. The present study uses the same model coefficients as described in the reference study, however, in that case the mix model was run in a Lagrange computation for the resolved flow and shock hydrodynamics.

Our results for parameter self-similarity and for mix width agree closely with the previous work [1] for RT unstable mixing and for turbulent decay in HIT (homogeneous isotropic turbulence), where in both cases, there is no significant mass averaged fluid flow. In the shock driven RM mix studies, as the mixing layer grows it must propagate across the computational mesh in the Eulerian implementation. There is a significant difference here and in the reference study between the mix growth rates, characterized as the power law exponent (θ) best fit to the mix width verses time in single shock RM tests. The model result in our Eulerian code implementation consistently yields θ values in the range ~ 0.35- 0.45 for RM instability mix, which is within the range of values reported in the literature, but higher than the value, $\theta \sim 0.25$, expected from a self-similarity analysis in the Lagrange frame as described in the reference study. These results are consistent with a relative insensitivity of the mix width to variations in the drag coefficient in the Eulerian framework. Additional tests reported here, with different values of an imposed uniform background (mass averaged) fluid velocity, suggest the difference may be related to early time differences in the turbulent kinetic energy, which arise from the Eulerian frame convective derivative in the K evolution equation.

Implications are that the model results are sensitive to the implementation details and the computational framework, in a Lagrangian or Eulerian computation. Different calibrations may apply to the model in Lagrange, Eulerian, or in ALE computations. The spreading of a shocked contact discontinuity due to numerics in an Eulerian frame is a well known issue. In RM mixing, the numerical spreading of the contact discontinuity must be distinguished from the spreading intended in the mix model. This is a significant and broad based challenge for mix modeling in an Eulerian code and lies beyond the specifics of the present mix model and implementation.

Sensitivity of the model in several areas was examined. Mix growth rates for RM are found to be sensitive to initial conditions (IC) and these IC differ from the model IC values used to match RT results. This sensitivity to IC suggests that a methodology should be developed to set the IC for a specific regime, especially in arbitrary acceleration combinations of RT (constant acceleration) and RM (impulsive acceleration). In comparison to re-shock experiments (Vetter-Sturtevant and Poggi,et.al.), we were able to obtain a good match to the first shock or to the re-shock growth rates but not both simultaneously with a single set of model parameters. Grid convergence for the K-L model in RT and in RM mixing is compared to convergence for a multi-fluid mix model in a species-pressure gradient driven mix test. Convergence for the K-L model is superior on course grids, and comparable on the finer grids. Varying the turbulent diffusivity coefficient near the default value of unity has a small influence on the mix width, but directly controls the 'atomically mixed fraction' even for very

small values of the diffusivity. The model output of fluid volume fractions and separately, the atomically mixed volume fractions per material, allows a rigorous approach in the calculation of reactivity in transient mixing fluids.

Acknowledgements

The authors acknowledge the support of PEM (Physics and Engineering Models) under ASC (Advanced Scientific Computing) and the direction of Guy Dimonte.

Appendix: K-L model equations with drag buoyancy source

This summary of the model equations are adapted directly from the reference article by Dimonte-Tipton [Phys. Fluids, 18, 085101 (2006)] denoted here as [DT].

The turbulence model modifies transport in the conservation equations for the mass average flow density, momentum, and internal energy as,

$$\frac{D\rho}{Dt} = -\rho\,\nabla\cdot u$$

$$\rho\frac{Du}{Dt} = -\nabla p - \nabla : \pi_{trb} - \nabla : q_{av} + \rho g$$

$$\rho\frac{De}{Dt} = -(p + q_{av})\nabla\cdot u + \nabla\cdot\left(\frac{\mu_T}{N_e}\nabla e\right) - S_K$$

with an equation for mass fraction, F_r, for species r, given by

$$\rho\frac{DF_r}{Dt} = \nabla\cdot\left(\frac{\mu_T}{N_F}\nabla F_r\right)$$

The mass averaged velocity, u, defines the convective derivative in each equation as

$$\frac{D()}{Dt} = \frac{\partial()}{\partial t} + u\cdot\nabla()$$

Artificial viscosity, q_{av}, can be a tensor quantity and must be defined consistently in the momentum equation and in the work term in the internal energy equation. This stabilizes the numerics and maintains the shock jump conditions in Lagrange, ALE, and Lagrange phase computational methods where energy conservation is expressed in an internal energy equation. This is not a feature of the K-L model, but the model must be compatible within this computational framework. The subscripted parameters, N_s, are turbulent diffusivity parameters set in [D-T] by self-similarity. Other variables have their usual meaning.

The transport equations are closed by relating the turbulent stress tensor, π_{trb}, and the turbulent diffusivity, μ_T, to the model parameters, K and L, respectively representing the turbulent kinetic energy and a turbulent scale length. The turbulent stress tensor,

$$\pi_{trb} = \frac{2}{3}\delta_{ij}\rho K - \mu_T\left(\nabla u + \nabla^T u - \frac{2}{3}\delta_{ij}\nabla\cdot u\right)$$

is approximated with a diagonal component in the form,

$$\pi_{trb} = \left(\frac{2}{3} + C'_p\right)\rho K$$

where the 2/3 derives from the usual diagonal form and the coefficient, C'_p, is an empirical adjustment to approximate the off-diagonal terms as described in [DT] (their C_p is our $(2/3 + C'_p)$). This approximation is derived in [33]. The default value for C'_p is zero.

The turbulent diffusivity, μ_T, is related to the model parameters, K and L, as

$$\mu_T = C_T \rho L (2K)^{1/2}$$

The equations used to evolve K and L are,

$$\rho\frac{DK}{Dt} = -\pi_{trb} : (\nabla u) + \nabla \cdot \left(\frac{\mu_T}{N_K}\nabla K\right) + S_K$$

$$\rho\frac{DL}{Dt} = \nabla \cdot \left(\frac{\mu_T}{N_L}\nabla L\right) + \rho(2K)^{1/2} + C_C \rho L \, \nabla \cdot u$$

The turbulent viscous heating, $-\pi_{trb} : (\nabla u)$, in the K equation is simplified in this model due to issues associated with numerical instabilities with shear in the presence of shocks, as discussed in [D-T]. Consistent with the simplified turbulent stress tensor described above, the turbulent viscous heating becomes

$$\pi_{trb} : (\nabla u) \approx (2/3)\rho K \, \nabla \cdot u$$

This restricts the model in its present form because it cannot be calibrated against the K-H or shear instability since the shear terms required to generate turbulent kinetic energy from the K-H instability are omitted.

The source term for the turbulent kinetic energy, S_K, is unique in the Dimonte-Tipton version of the K-L model, and is written to explicitly represent the buoyancy and drag terms familiar in the R-T and R-M mix community,

$$S_K = \rho(2K)^{1/2}\left[C_B A \, g - C_D \frac{2K}{L}\right]$$

where the coefficients for buoyancy, C_B, and for drag, C_D, are set in comparison to empirical data. The Atwood number, A, is calculated as a local quantity within the computation using,

$$A = \frac{\rho_+ - \rho_-}{\rho_+ + \rho_-} + C_A \frac{L}{\rho + L\,|\partial\rho/\partial x|} \frac{\partial\rho}{\partial x}$$

as described in detail and justified in [DT]. The model coefficient, C_A, is introduced to scale the second term contribution to A.

References

[1] G. Dimonte, R. Tipton, "K-L turbulence model for self-similar growth of the Rayleigh-Taylor and Richtmyer-Meshkov instabilities", Phys. Fluids, 18, 085101 (2006).

[2] C-J Chen and S-Y Jaw, Fundamentals of Turbulence Modeling, Taylor and Francis, Washington, DC 1998.

[3] B. Cheng, "Review of turbulent mixing models", AMS 29B(6):1703-1720 (2009).

[4] K. I. Read, "Experimental investigation of turbulent mixing by Rayleigh-Taylor instability," Physica D **12**, 45 1984.

[5] G. Dimonte and M. Schneider, "Turbulent Rayleigh-Taylor instability experiments with variable acceleration," Phys. Rev. E **54**, 3740 (1996).

[6] G. Dimonte and M. Schneider, "Density ratio dependence of Rayleigh-Taylor mixing for sustained and impulsive accelerations," Phys. Fluids **12(2)**, 304 (2000).

[7] Lord Rayleigh, "Investigation of the character of the equilibrium of an incompressible heavy fluid of variable density", p. 200 in *Scientific Papers II* Cambridge University Press, Cambridge, 1900, reprinted by Dover, New York, NY, 1964.

[8] G. I. Taylor, "The instability of liquid surfaces when accelerated in a direction perpendicular to their plane," Proc. R. Soc. London, Ser. A **201**, 192 1950.

[9] R. D. Richtmyer, "Taylor instability in shock acceleration of compressible fluids," Commun. Pure Appl. Math. **13**, 297 1960.

[10] E. E. Meshkov, "Instability at interface of two gases when accelerated by shock waves", Izv. Acad. Sci. USSR Fluid Dyn. **4**, 101 1969.

[11] M. Vetter and B. Sturtevant, "Experiments on the Richtmyer-Meshkov instability of an air/SF6 interface," Shock Waves **4**, 247 1995.

[12] F. Poggi, M.-H. Thorembey, and G. Rodriguez, "Velocity measurements in turbulent gaseous mixtures induced by Richtmyer-Meshkov instability," Phys. Fluids **10**, 2698 1998.

[13] D. L. Youngs, "Numerical simulation of turbulent mixing by Rayleigh-Taylor instability", Physica D **12**, 32, 1984.

[14] G. Dimonte, D. L. Youngs, A. Dimits, S. Weber, M. Marinak, S. Wunsch, C. Garasi, A. Robinson, M. J. Andrews, P. Ramaprabhu, A. C. Calder, B. Fryxell, J. Biello, L. Dursi, P. MacNeice, K. Olson, P. Ricker, R. Rosner, F. Timmes, H. Tufo, Y.-N. Young,

and M. Zingale, "A comparative study of the turbulent Rayleigh-Taylor instability using high-resolution three dimensional numerical simulations: The Alpha-Group collaboration," Phys. Fluids **16**, 1668 2004.

[15] D. Oron, L. Arazi, D. Kartoon, A. Rikanati, U. Alon, and D. Shvarts, "Dimensionality dependence of Rayleigh-Taylor and Richtmyer-Meshkov instability late-time scaling laws," Phys. Plasmas **8**, 2883 (2001).

[16] U. Alon, J. Hecht, D. Ofer, and D. Shvarts, "Power laws and similarity of Rayleigh-Taylor and Richtmyer-Meshkov mixing fronts at all density ratios", Phys. Rev. Lett. **74**, 534 (1995).

[17] J.O. Heinz, Turbulence, 2nd ed., McGraw-Hill, New York, NY 1975.

[18] G. L. Brown and A. Roshko, "On density effects and large structure in turbulent mixing layers," J. Fluid Mech. **64**, 775 (1974).

[19] V. Chiravalle, "The k-L turbulence model for describing buoyancy-driven fluid instabilities", Laser and Particle Beams, 24, 381 (2006).

[20]] D. Besnard, F. H. Harlow, R. M. Rauenzahn, and C. Zemach, "Turbulence transport equations for variable-density turbulence and their relation to two-field models," Los Alamos National Laboratory Report No. LA-12303-MS. Los Alamos, NM (1992).

[21] J.D. Schwarzkopf, R.A. Gore, and R.M.Rauenzahn, "Modelling anisotropy in turbulent mix", presented at NECDC conference, Los Alamos, 2010, Los Alamos Unclassified Report, LA-UR-10-06487, Los Alamos, NM (2010).

[22] Guy Dimonte, personal communication, Los Alamos National Laboatorty, Los Alamos, NM (2009).

[23] A.J. Scannapieco, personal communication, Los Alamos National Laboatorty, Los Alamos, NM (2007).

[24] D.L. Youngs, "The Lagrangian re-map method ", in Implicit Large Eddy Simulations, eds. Grinstein, F.F., Margolin, L.G., Ryder, W.J., Cambridge University Press, New York (2007).

[25] R. L.Bowers and J. R. Wilson, Numerical Modeling in Applied Physics and Astrophysics, Jones and Barlett, Boston (1991).

[26] J.I. Castor, Radiation Hydrodynamics, Cambridge University Press, New York, 2004.

[27] D.L. Youngs, "Time-dependent multi-material flow with large fluid distortion",

in Numerical Methods for Fluid Dynamics, eds., K.W. Morton and M.J. Barnes, 273-85 Academic Press, New York (1982).

[28] F.H. Harlow and A.A. Amsden, "Fluid Dynamics", Los Alamos National Laboratory Report, LA-4700, Los Alamos, NM 1971.

[29] D.J. Hill, C Pantano, D. Pullin, "Large-eddy simulation and multiscale modeling of a Richtmyer-Meshkov instability with reshock", J. Fluid Mech. 557, 29-61 (2006).

[30] S. Barre, D. Alem, and J. P. Bonnet, "Experimental study of a normal shock/homogeneous turbulence interaction," AIAA J. **34**, 968 1996.

[31] A. J. Scannapieco and B. L. Cheng, "A multifluid interpenetration model," Phys. Lett. A **299**, 49 2002.

[31] E.L.Vold and A.J. Scannpieco, "A sub-grid volume of fluids (VOF) model for mixing in resolved scale and in unresolved scale computations", Los Alamos National Laboratory report, LA-UR-07-0302, Los Alamos, NM (2007).

[33] K. Sinha, K. Mahesh, and G. V. Candler, "Modeling shock unsteadiness in shock/turbulence interaction," Phys. Fluids **15**, 2290 (2003).

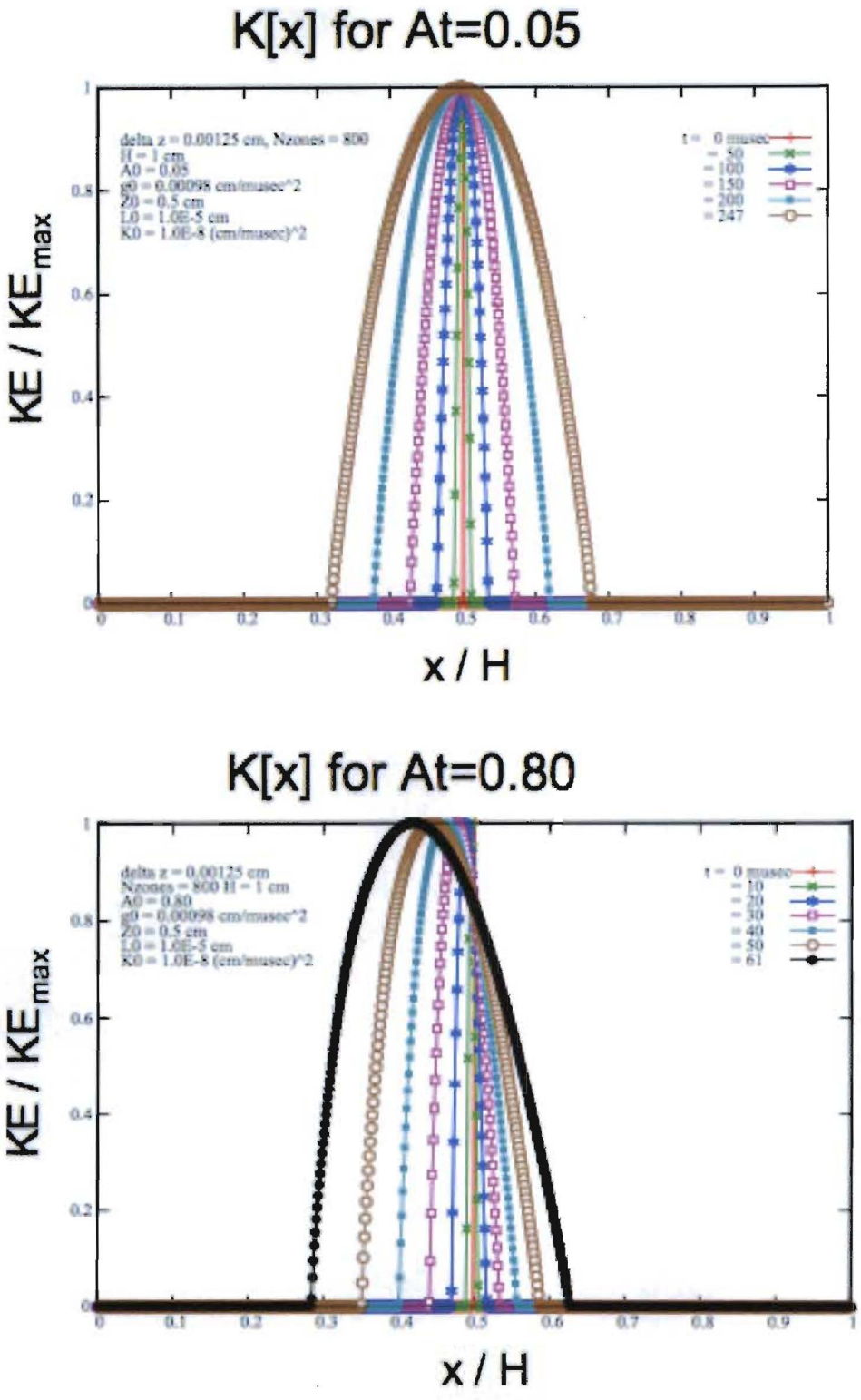

Figure 1. Model kinetic energy, normalized at select times during R-T instability mixing showing the self-similar growth for low Atwood number (0.05) and high Atwood number (0.8) cases.

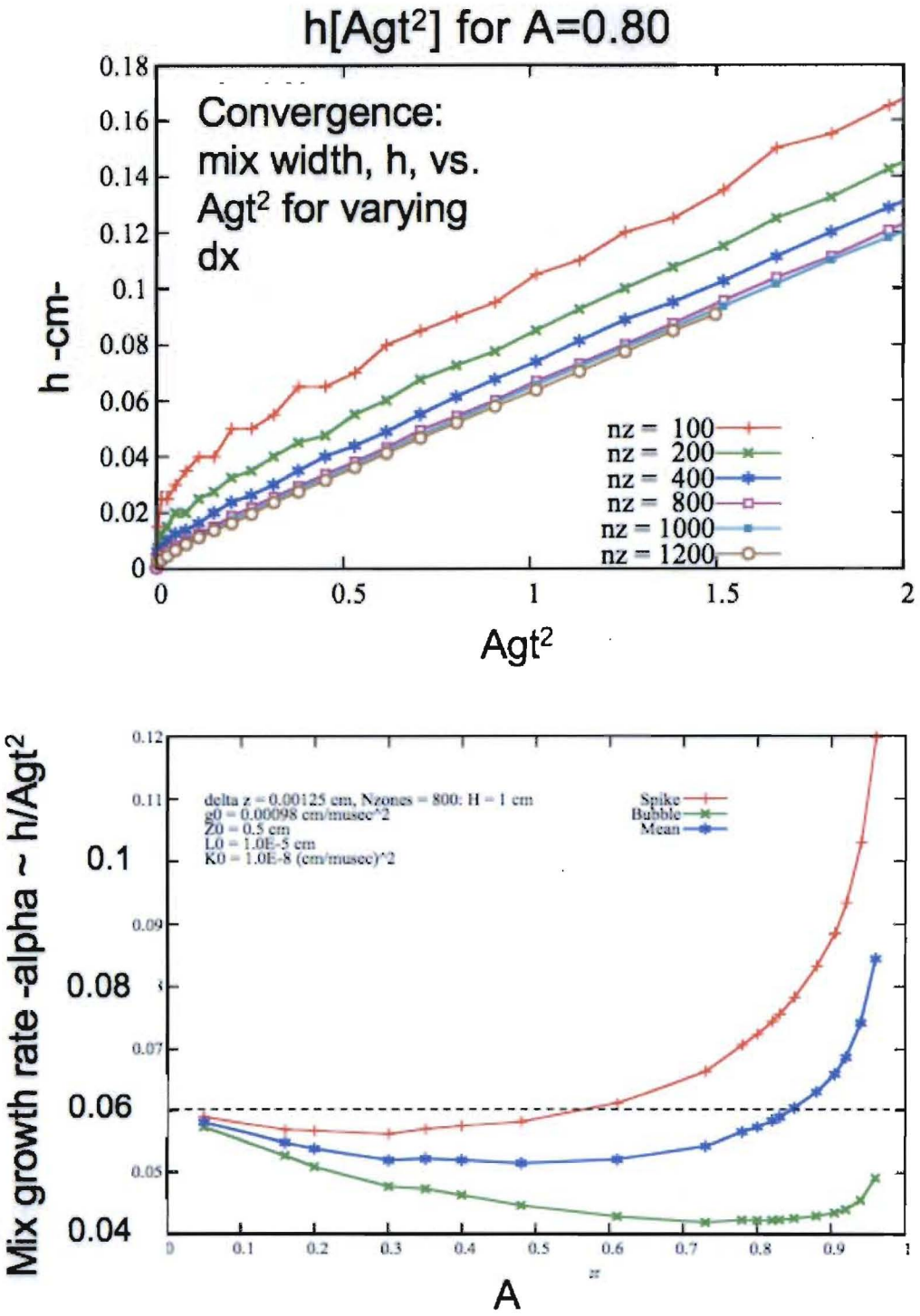

Figure 2. (Top) Mix width verses scaled distance, Agt^2, for the model results in R-T instability, showing convergence for results by refining the grid (number of zones = nz = 1/dx). The bottom panel shows the resulting R-T growth rate, alpha, $\alpha = h / Agt^2$, verses Atwood number, A.

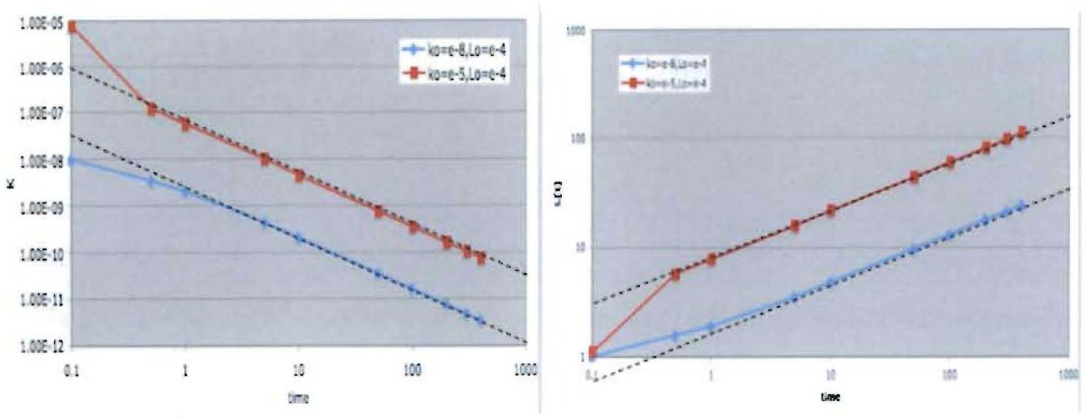

Figure 3. Turbulent kinetic energy, K, (left) and turbulent scale length, L, (right panel) verses time on log-log plots showing, respectively, power law decay and growth during the decay of homogeneous isotropic turbulence (HIT) for two initial conditions of $K = K_o$.

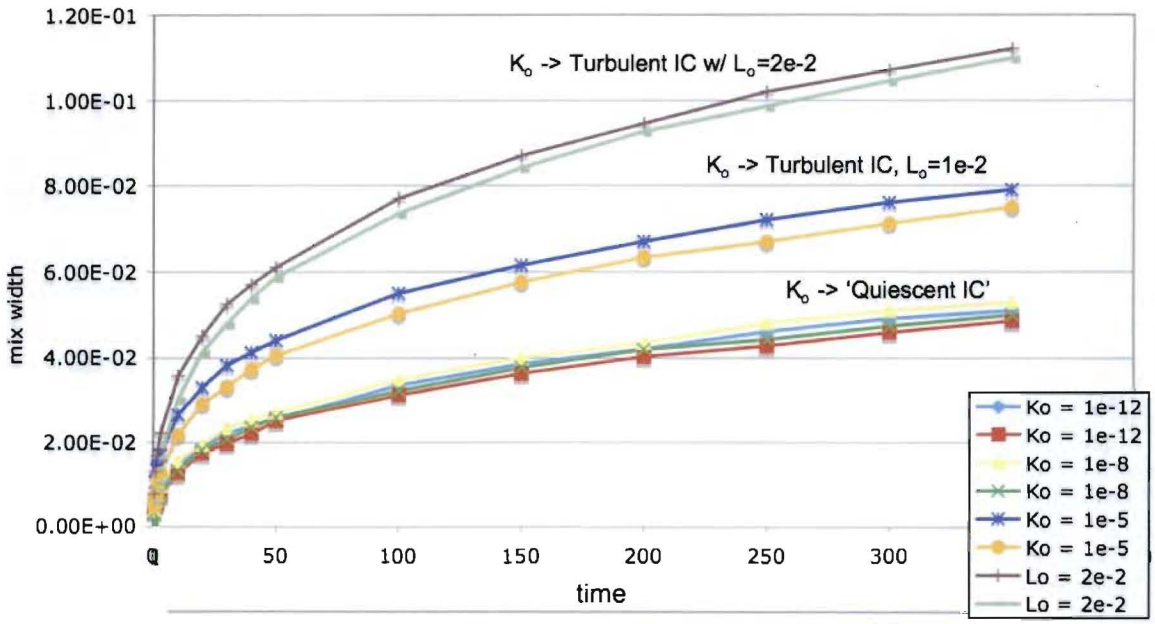

Figure 4. Mix width verses time showing sensitivity of results to initial conditions (IC) for select RM cases. Curves for spike and for bubble mix are shown separately for each set of IC, where the spike growth is slightly greater than bubble growth in each case. 'Quiescent' and 'turbulent' IC labels are described further in the text.

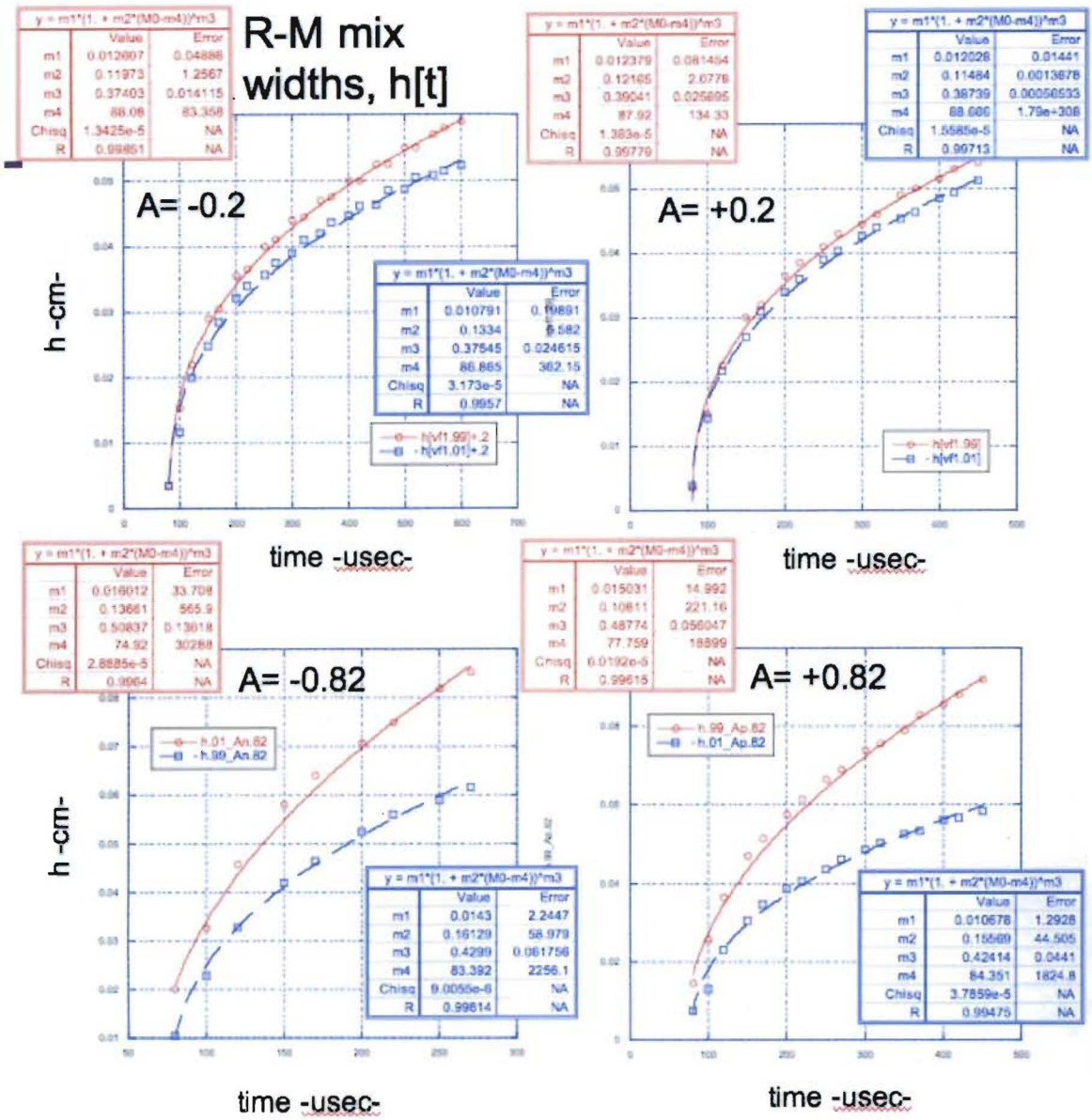

Figure. 5. Mix widths verses time for the basic single shock RM instability using four different values of the Atwood number, A. Spike mix widths are shown in red and bubble mix widths are in blue. Negative A indicates a drop in density as the shock crosses the initial discontinuity, and positive A is an increase in density as seen by the incoming shock. Curve fits are described in the text.

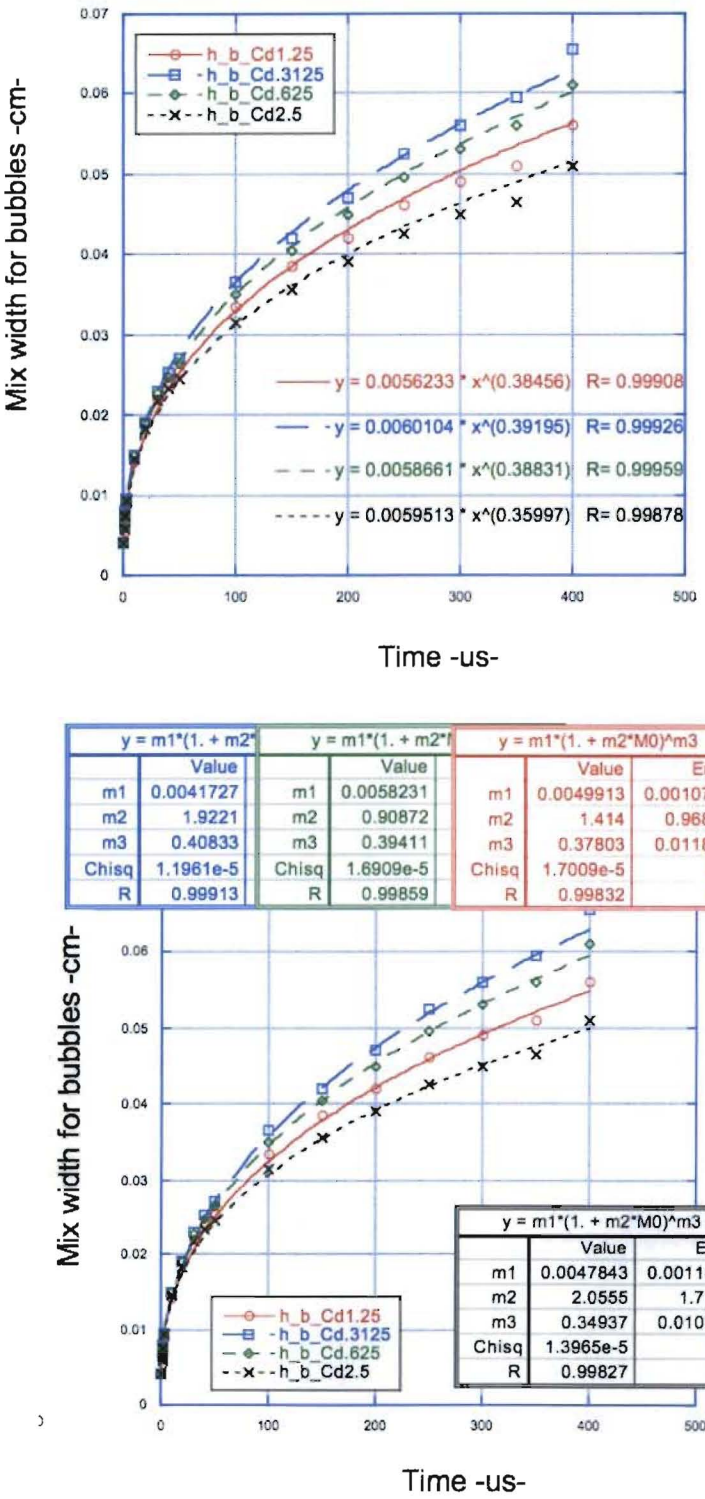

Fig. 6 Mix width verses time for varying drag coefficient, C_D, showing the two parameter power law fits (top panel) to model results (symbols), and the three parameter power law fits (bottom panel) to model results.

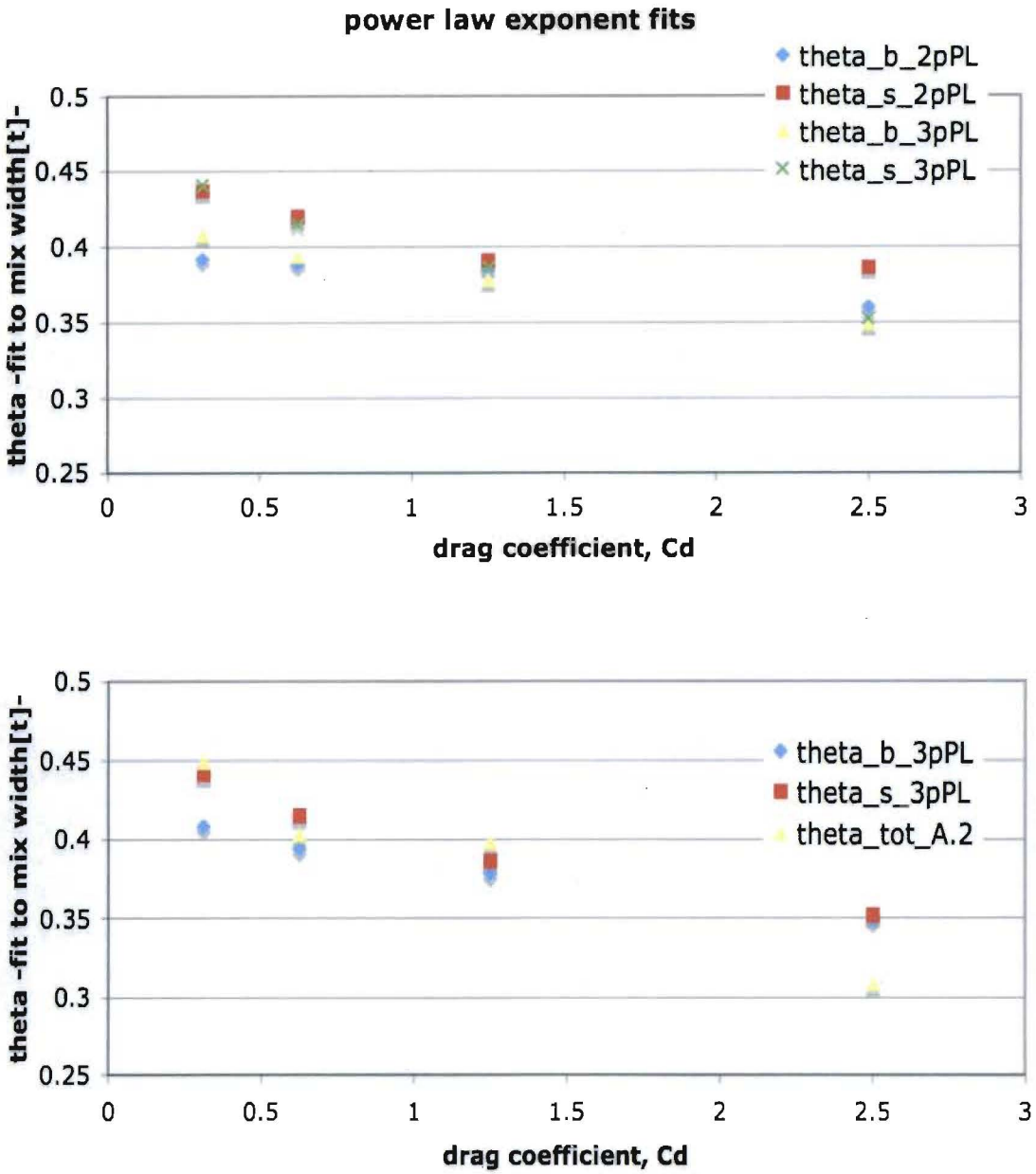

Figure 7. Theta, θ, obtained as the best fit power law exponent to the model result for the mix width, h, verses time, is shown verses the model drag coefficient. The top figure compares results for the two and three parameter power law fits from Fig.6, and the lower figure compares results for spikes and bubbles in a long duration mixing test and for total mix width in a shorter duration test (see text).

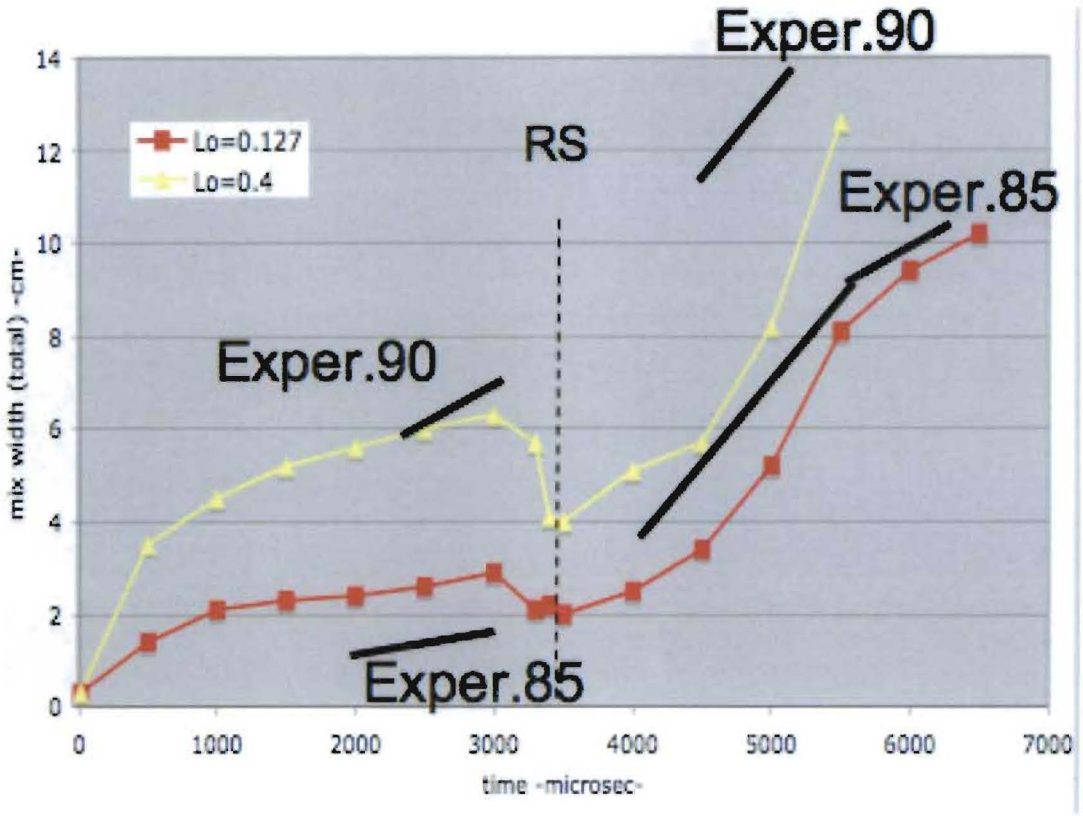

Figure 8. Mix model results are compared to experimental data from the Vetter-Sturtevant re-shock experiment [11]. Heavy dark lines indicate experimental data for two similar experiments (85 and 90), and the lines with symbols show mix model results for two parameter settings described in the text.

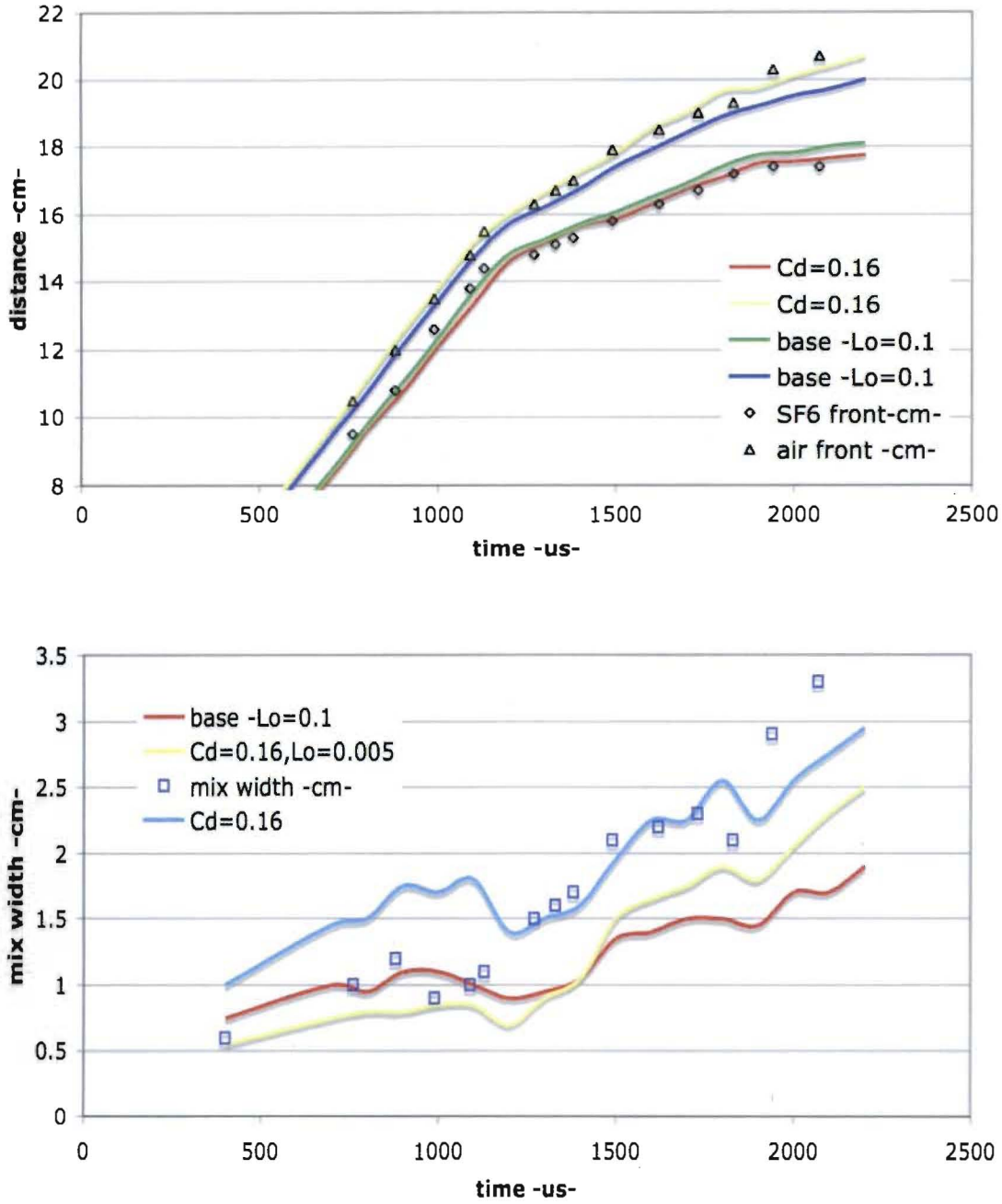

Figure 9. Mix model results are compared to experiment for the Poggi, et.al. re-shock experiments [12]. Top figure shows mix front positions as given in the Poggi paper, for two model settings (lines) and for select experimental data (symbols). The bottom figure converts the mix front positions to mix widths, allowing a more detailed comparison between model results and these experimental data points.

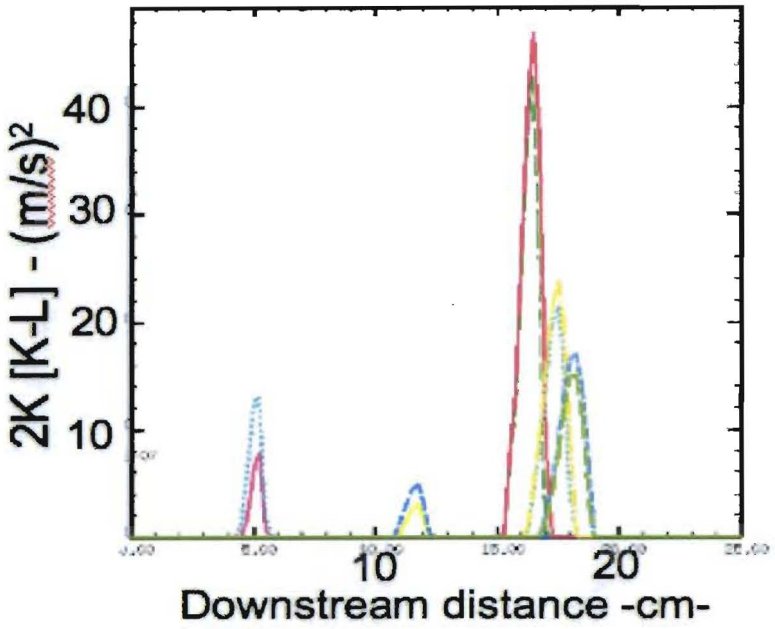

Figure 10. Turbulent kinetic energy levels, given as 2K, from the mix model at downstream locations for comparison to the experimental data in Poggi, et.al. [12].

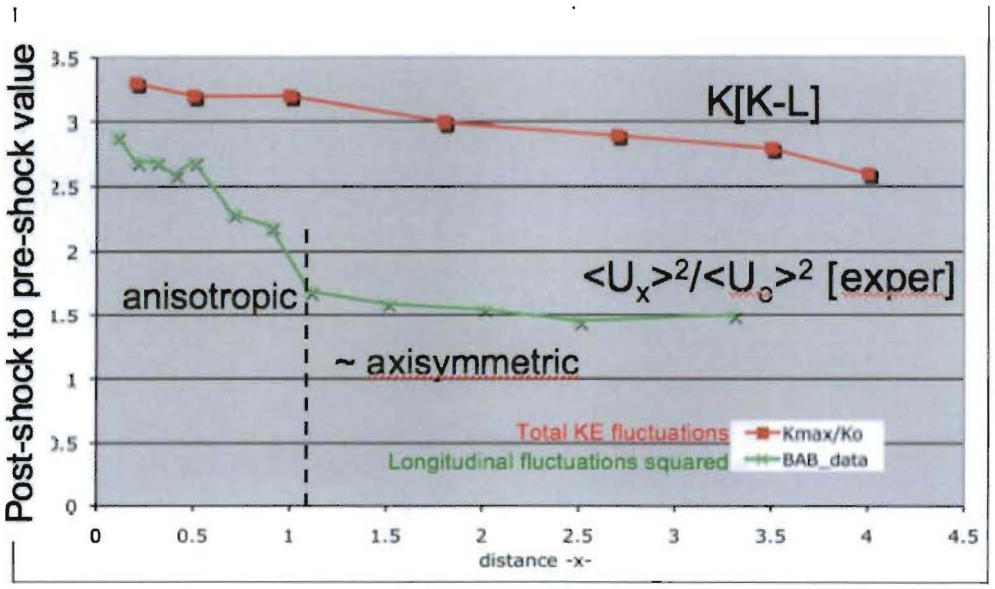

Figure 11. Shock amplification of turbulent kinetic energy in the mix model, K[K-L], compared to experimental data by Barre, et.al. (denoted BAB [30]) of the longitudinal turbulent fluctuations during anisotropic decay.

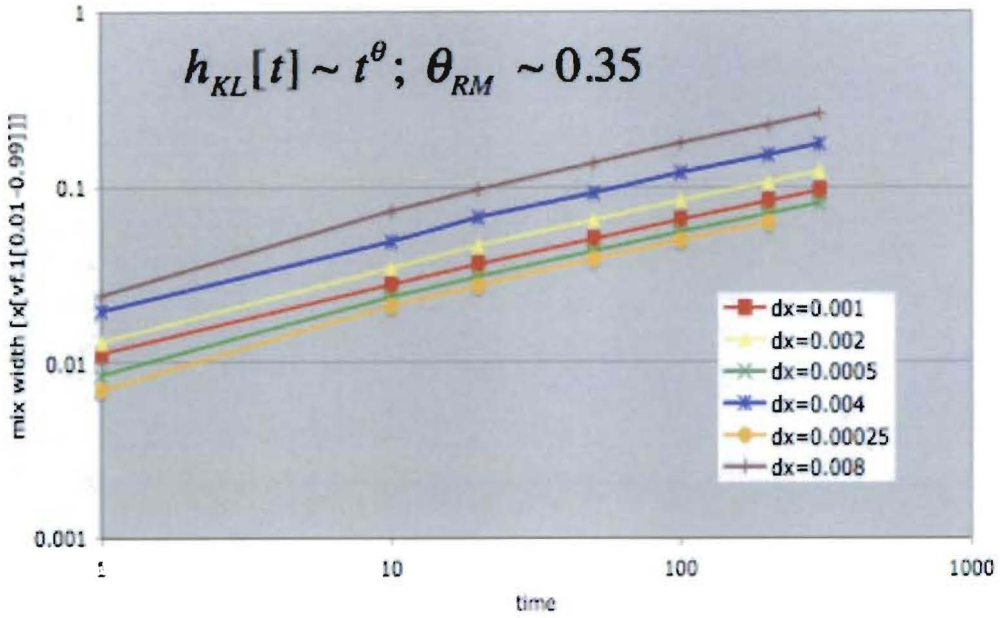

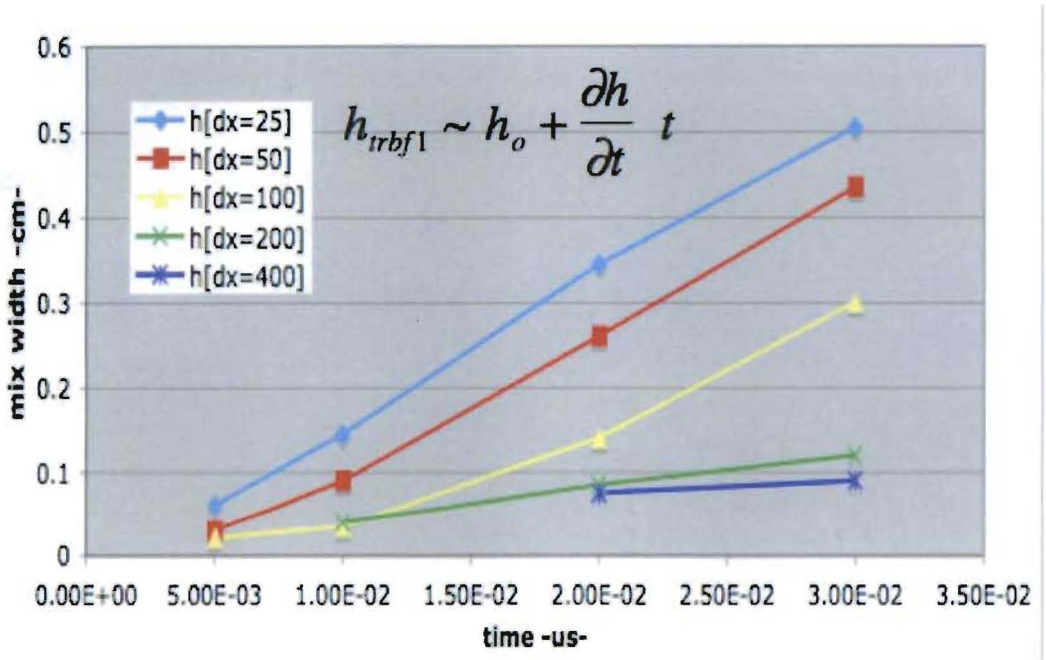

Figure 12. Grid convergence studies for mix models. (Top panel) Convergence for the K-L mix model in a R-M single shock test problem. For comparison, (bottom panel) convergence of a multi-fluid interpenetration mix model [Scannapieco and Cheng, 2002] is shown for an interfacial pressure gradient driven mix problem, as described in the text.

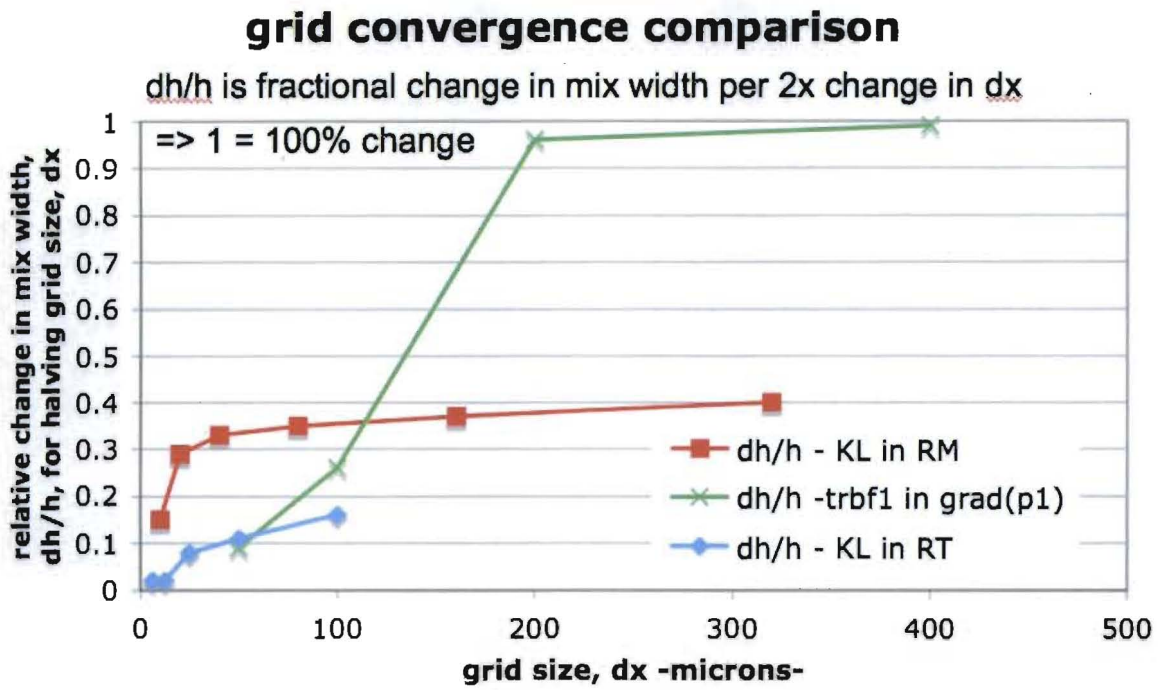

Figure 13. Grid convergence comparison between the K-L model results for an RT problem (taken from Fig. 2A), the K-L results for RM problems (from Fig.12 top) and the interpenetration model of Scannapieco and Cheng in the pressure gradient driven mix problem (taken from Fig.12 bottom, and labeled here as 'trbf1 in grad(p1)'). The results are plotted as the fractional change in mix width resulting from a refinement in the mesh resolution by a factor of two.

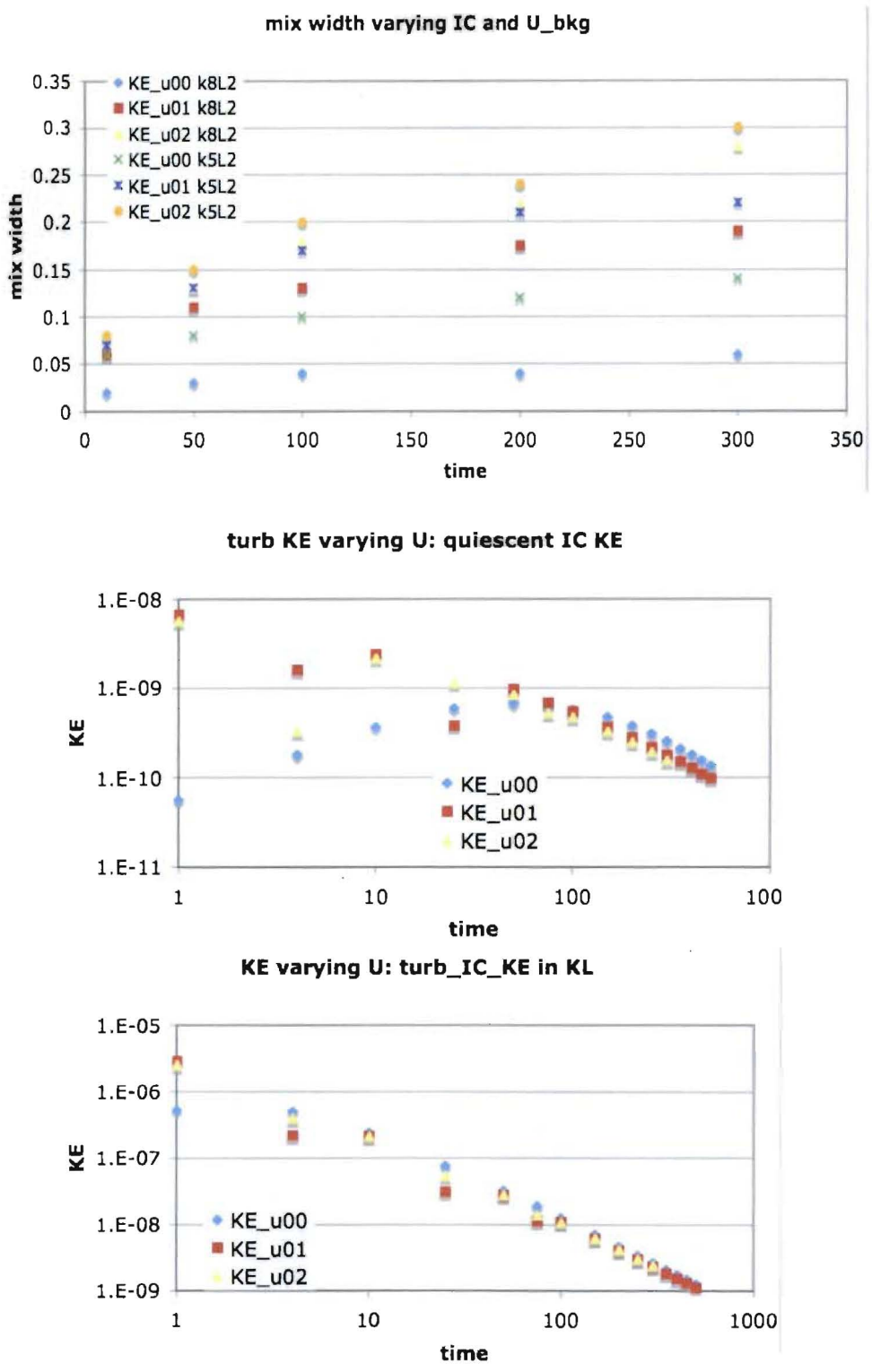

Figure 14. Model results for mix width in time (top panel) due to variations in a uniform background flow speed and for two initial condition (IC) values for K_o. Model turbulent kinetic energy (K) verses time for the different background flow speeds, shown separately for the two IC values for K_o (bottom two panels).

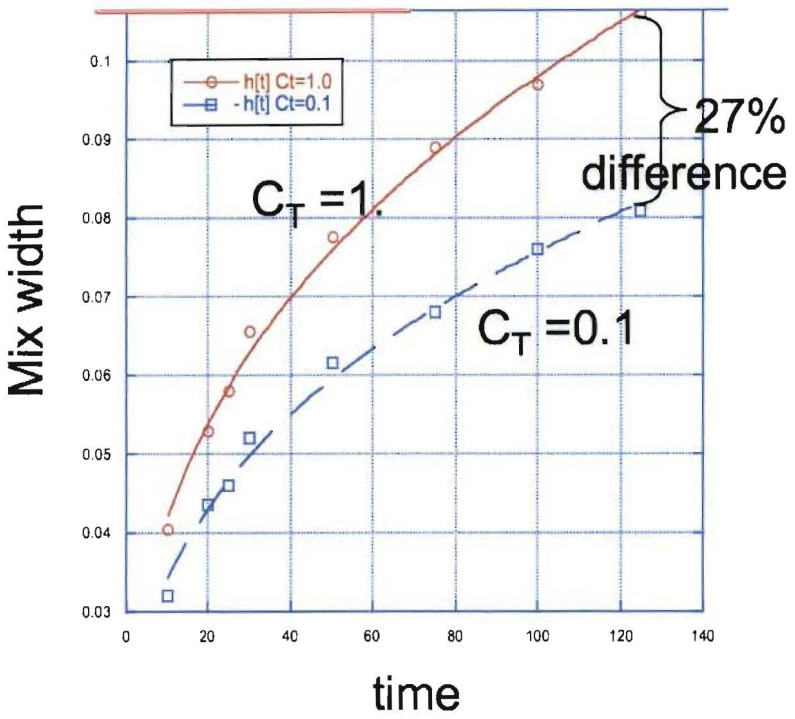

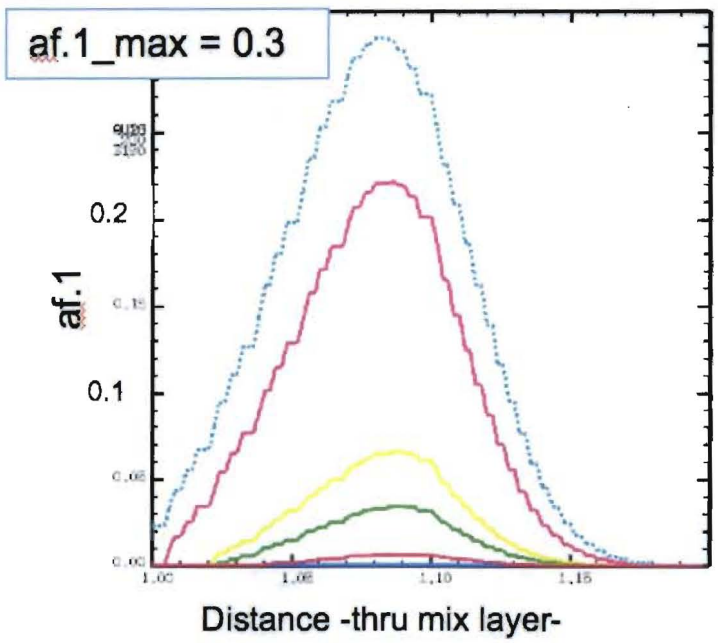

Figure 15. Mix width verses time (top panel) for two values (C_T = 1, 0.1) of the model coefficient multiplying turbulent diffusivity, C_T. Atomically mixed fraction (bottom panel) of the heavier fluid across the mix layer for five values of the turbulent diffusivity coefficient in decreasing sequence for C_T = 1, 0.5, 0.1, 0.05, and 0.01. This is discussed in the text in comparison to mix width.

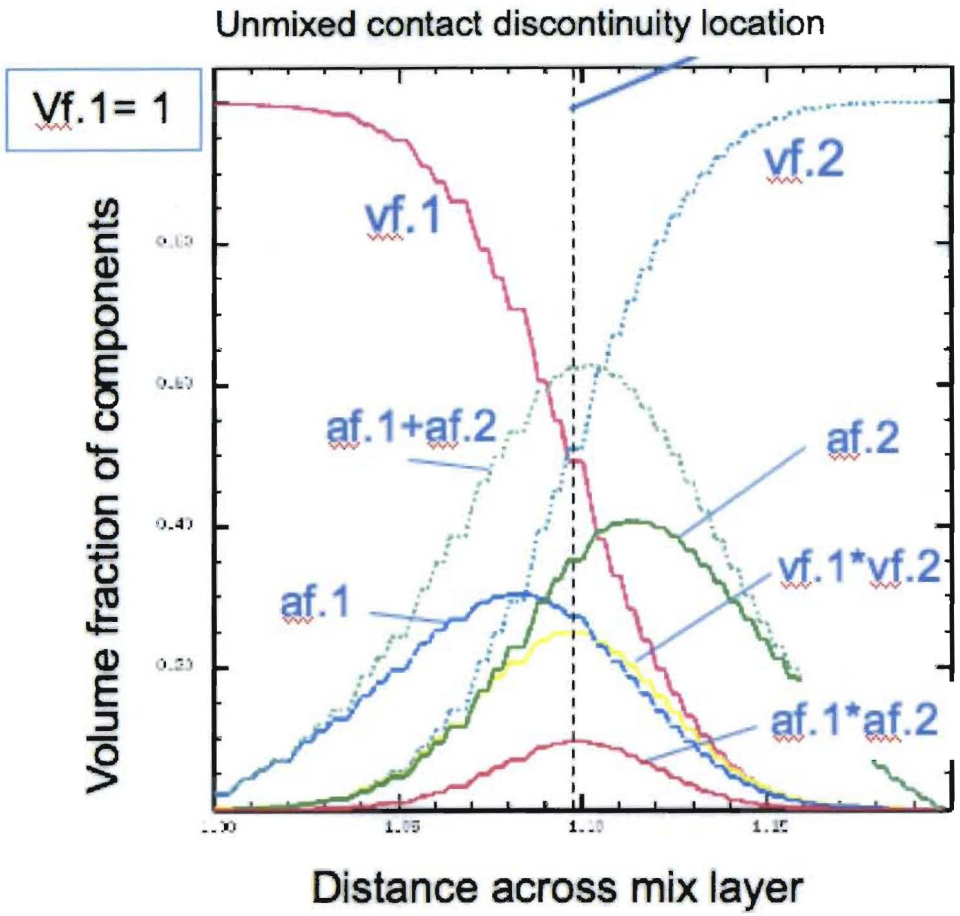

Figure 16. Comparison of the total volume fractions (vf) and the atomically mixed fractions (af) for the two fluids (.1 and .2) across the mix layer in a typical RM problem calculated in the Eulerian code implementation. These are discussed in the text.